

# Evolving GPU Machine Code

**Cleomar Pereira da Silva**

CLEOMAR.SILVA@IFC-VIDEIRA.EDU.BR

*Department of Electrical Engineering*

*Pontifical Catholic University of Rio de Janeiro (PUC-Rio)*

*Rio de Janeiro, RJ 22451-900, Brazil*

*Department of Education Development*

*Federal Institute of Education, Science and Technology - Catarinense (IFC)*

*Videira, SC 89560-000, Brazil*

**Douglas Mota Dias**

DOUGLASM@ELE.PUC-RIO.BR

*Department of Electrical Engineering*

*Pontifical Catholic University of Rio de Janeiro (PUC-Rio)*

*Rio de Janeiro, RJ 22451-900, Brazil*

**Cristiana Bentes**

CRIS@ENG.UERJ.BR

*Department of Systems Engineering*

*State University of Rio de Janeiro (UERJ)*

*Rio de Janeiro, RJ 20550-013, Brazil*

**Marco Aurélio Cavalcanti Pacheco**

MARCO@ELE.PUC-RIO.BR

*Department of Electrical Engineering*

*Pontifical Catholic University of Rio de Janeiro (PUC-Rio)*

*Rio de Janeiro, RJ 22451-900, Brazil*

**Leandro Fontoura Cupertino**

FONTOURA@IRIT.FR

*Toulouse Institute of Computer Science Research (IRIT)*

*University of Toulouse*

*118 Route de Narbonne*

*F-31062 Toulouse Cedex 9, France*

**Editor:** Una-May O'Reilly

## Abstract

Parallel Graphics Processing Unit (GPU) implementations of GP have appeared in the literature using three main methodologies: (i) *compilation*, which generates the individuals in GPU code and requires compilation; (ii) *pseudo-assembly*, which generates the individuals in an intermediary assembly code and also requires compilation; and (iii) *interpretation*, which interprets the codes. This paper proposes a new methodology that uses the concepts of quantum computing and directly handles the GPU machine code instructions. Our methodology utilizes a probabilistic representation of an individual to improve the global search capability. In addition, the evolution in machine code eliminates both the overhead of compiling the code and the cost of parsing the program during evaluation. We obtained up to 2.74 trillion GP operations per second for the 20-bit Boolean Multiplexer benchmark. We also compared our approach with the other three GPU-based acceleration methodologies implemented for quantum-inspired linear GP. Significant gains in performance were obtained.

**Keywords:** genetic programming, graphics processing units, machine code.

## 1. Introduction

Genetic programming (GP) is a metaheuristic method to automatically generate computer programs or key subcomponents (Banzhaf et al., 1997; Koza, 1992; Poli et al., 2008). Its functionality is based on the Darwinian principle of natural selection, in which a population of computer programs, or individuals, is maintained and modified based on genetic variation. The individuals are then evaluated according to a fitness function to reach a better solution. GP has been successfully applied to a variety of problems, such as automatic design, pattern recognition, robotic control, data mining, and image analysis (Koza, 1992, 1994; Tackett, 1993; Busch et al., 2002; Harding and Banzhaf, 2008; Langdon, 2010a). However, the evaluation process is time consuming. The computational power required by GP is enormous, and high-performance techniques have been used to reduce the computation time (Andre and Koza, 1996; Salhi et al., 1998). GP parallelism can be exploited on two levels: multiple individuals can be evaluated simultaneously, or multiple fitness cases for one individual can be evaluated in parallel. These approaches have been implemented in multiprocessor machines and computer clusters (Page et al., 1999; Turton et al., 1996; Bennett III et al., 1999).

The recent emergence of general-purpose computing on Graphics Processing Units (GPUs) has provided the opportunity to significantly accelerate the execution of many costly algorithms, such as GP algorithms. GPUs have become popular as accelerators due to their high computational power, low cost, impressive floating-point capabilities, and high memory bandwidth. These characteristics make them attractive platforms to accelerate GP computations, as GP has a fine-grained parallelism that is suitable for GPU computation.

The power of the GPU to accelerate GP has been exploited in previous studies. We divide these efforts into three main methodologies: (i) *compilation* (Chitty, 2007; Harding and Banzhaf, 2007, 2009; Langdon and Harman, 2010); (ii) *pseudo-assembly* (Cupertino et al., 2011; Pospichal et al., 2011; Lewis and Magoulas, 2011); and (iii) *interpretation* (Langdon and Banzhaf, 2008a; Langdon and Harrison, 2008; Robilliard et al., 2009; Wilson and Banzhaf, 2008). In the *compilation* methodology, each evolved program, or GP individual, is compiled for the GPU machine code and then evaluated in parallel on the GPU. In the *pseudo-assembly* methodology, the individuals are generated in the pseudo-assembly code of the GPU, and a just-in-time (JIT) compilation is performed for each individual to generate the GPU machine code, which is evaluated in parallel on the GPU. In the *interpreter* methodology, an interpreter that can run programs immediately is used. The individuals are evaluated in parallel on the GPU.

These methodologies have been used with varying levels of success, and they have different advantages and disadvantages. In the *compilation* methodology, the GPU's fine-grain parallelism can be exploited by evaluating multiple individuals and multiple fitness cases simultaneously. However, the time spent compiling each GP individual influences the performance results considerably, making the GPU compiler decidedly slow. The compilation process in a GPU involves a series of steps. When GP needs to evaluate millions of programs, spending a few seconds to compile a single CUDA program becomes a large obstacle to producing a solution within a reasonable period of time. The *pseudo-assembly* methodology can also exploit multiple individuals and multiple fitness case evaluations in parallel. A pseudo-assembly code can be compiled several hundred times faster than an original GPU

code, allowing large data sets to be considered. Nevertheless, the programs still need to be compiled, and the compilation time must be considered as part of the overall GP process. The *interpreter* methodology differs from the *compilation* methodology in that the interpreter is compiled once and reused millions of times. This approach eliminates the compilation overhead but includes the cost of parsing the evolved program. The *interpreter* methodology typically works well for shorter programs and smaller training cases.

In this work, we propose a new methodology for using GPUs in the GP evolution process. We used a quantum-inspired evolutionary algorithm (QEA) that handles the instructions of the GPU machine code directly. QEAs represent one of the most recent advances in evolutionary computation (Zhang, 2011). QEAs are based on quantum mechanics, particularly the concepts of the quantum bit and the superposition of states. QEAs can represent diverse individuals in a probabilistic manner. By this mechanism, QEAs offer an evolutionary mechanism that is different and, in some situations, more effective than traditional evolutionary algorithms. The quantum probabilistic representation reduces the number of chromosomes required to guarantee adequate search diversity. In addition, the use of quantum interference provides an effective approach to achieve fast convergence to the best solution due to the inclusion of an individual's past history. It offers a guide for the population of individuals that helps to exploit the current solution's neighborhood.

Our methodology is called GPU machine code genetic programming, **GMGP**, and is based on linear genetic programming (LGP) (Nordin, 1998; Brameier and Banzhaf, 2007; Oltean et al., 2009). In LGP, each program is a linear sequence of instructions. LGP is the most appropriate for machine code programs, as computer architectures require programs to be provided as linear sequences. Computers do not naturally run tree-shaped programs. Tree-based GP must employ compilers or interpreters (Poli et al., 2008).

GMGP performs the evolution by modifying the GPU machine code, thus eliminating the time spent compiling the individuals while also avoiding the interpretation overhead. The individuals are generated on the CPU, and the individuals are evaluated in parallel on the GPU. The evaluation process is performed with a high level of parallelism: individuals are processed in parallel, and the fitness cases are simultaneously evaluated in parallel. Figure 1 illustrates the GPU-accelerated GP methodologies.

We compared our quantum-inspired methodology with the previous attempts to accelerate GP using GPUs. Our comparison considered the *compilation*, *pseudo-assembly*, and *interpretation* methodologies. We implemented these three methodologies to conform with linear GP and quantum-inspired algorithms, and to provide fair comparisons. GMGP outperformed all of these methodologies. The gains over *compilation* and *pseudo-assembly* originated from the elimination of the compilation time. The gains over *interpretation* originated from two sources. The first was the lack of the on-the-fly interpretation overhead. The second was the high number of comparison and jump instructions required by the interpreter, which produces serialization in the GPU execution. The main obstacle faced by GMGP was that the GPU machine code is proprietary, and the GPU's manufacturers do not provide any documentation for it. To solve this problem, we had to use reverse engineering to disassemble a series of GPU binary codes and determine the opcodes of the relevant instructions.

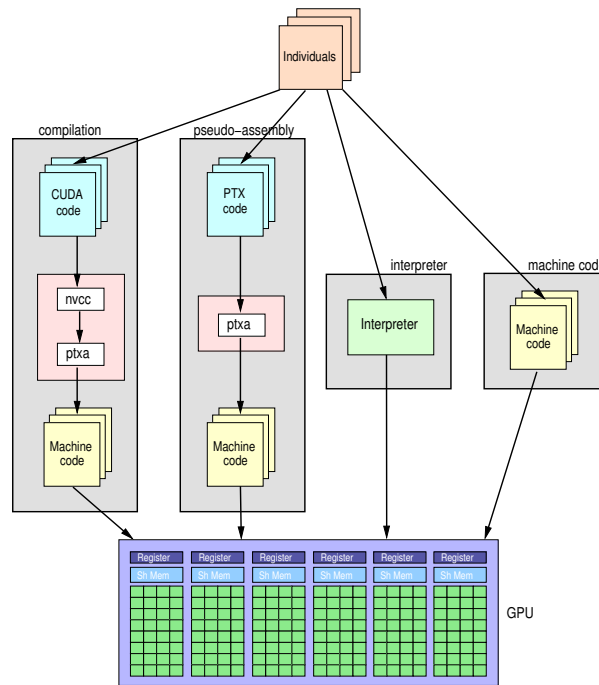


Figure 1: The different GP methodologies for GPU, considering the Nvidia technology. In the compilation methodology, a CUDA kernel is generated from each individual. The kernels are compiled in two main steps using the *nvcc* and *ptxas* compilers. In the pseudo-assembly methodology, pseudo-assembly codes (PTX) are generated from each individual and compiled using the *ptxas* compiler. In the interpreter methodology, each individual’s information is used by the interpreter to execute the program. The proposed machine code methodology generates a machine code program directly from each individual.

## 2. Related Work

Several approaches to accelerate GP on GPUs have been proposed in the literature. Harding and Banzhaf (2007) and Chitty (2007) were the first to present GP implementations on a GPU. Both works proposed compiler methodologies using tree-based GP. They obtained modest performance gains when small fitness cases were tested due to the overhead of transferring data to the GPU. Considerable performance gains were obtained for larger problems and when the compiled GP program was run many times.

Langdon and Banzhaf (2008a) were the first to propose an interpreter methodology. Their methodology used a tree-based GP and evaluated the entire population at once. Parallelism was exploited at the individual level, whereas the fitness cases were processed sequentially. Their technique was called the SIMD interpreter for GP, and they used conditional instructions to select opcodes, which can increase the overhead with the size of

the function set. The experimental results indicated moderate speedups but demonstrated performance gains even for very small programs. The same GPU SIMD interpreter was used by Langdon and Harrison (2008), who successfully applied GP to predict the breast cancer survival rate beyond ten years.

Robilliard et al. (2009) also studied the interpreter methodology, with a focus on avoiding the overhead of conditional instructions when interpreting the entire population at once. They proposed an interpreter that evaluates each GP individual on a different thread block. Each thread block was mapped to a different GPU multiprocessor during execution, avoiding branches. Inside the thread block, all threads executed the same instruction over different data subsets. Their results indicated performance gains compared to the methodology proposed by Langdon and Banzhaf (2008a).

Harding and Banzhaf (2009) studied the compilation methodology. A cluster of GPUs was used to alleviate the program compilation overhead. The focus was on processing very large data sets by using the cluster nodes to compile the GPU code and execute the programs. Different combinations of compilation and execution nodes could be used. The project was developed to run on a multi-platform Windows/Linux cluster and used low-end GPUs. Speedups were obtained for very large data sets. However, the use of high-end GPUs did not necessarily lead to better results, as the primary bottleneck remained in the compilation phase.

Langdon and Harman (2010) used the compilation methodology to automatically create an Nvidia CUDA kernel. Numerous simplifications were employed, such as not evolving the shared memory and threading information. The best evolved parallel individual was capable of correct calculations, proving that it was possible to elaborate a methodology to evolve parallel code. However, it was not possible to automatically verify the speedup obtained compared to the sequential CPU version, and the compilation still remained the bottleneck.

Wilson and Banzhaf (2008) implemented an LGP for GPU using the interpreter methodology on a video game console. In a previous work (Cupertino et al., 2011), we proposed a pseudo-assembly methodology, a modified LGP for GPU, called quantum-inspired linear genetic programming on a general-purpose graphics processing unit (QILGP3U). The individual was created in the Nvidia pseudo-assembly code, PTX, and compiled for evaluation through JIT. Dynamic or JIT compilation is performed in runtime and transformed the assembly code to machine code during the execution of the program. Several compilation phases were eliminated, and significant speedups were achieved for large data sets. Pospichal et al. (2011) also proposed a pseudo-assembly methodology with the evolution of PTX code using a grammar-based GP that ran entirely on the GPU.

The compilation time issue was addressed in a different manner by Lewis and Magoulas (2011). All population individuals were pre-processed to identify their similarities, and all of these similarities were grouped together. In this manner, repetitive compilation was eliminated, thus reducing the compilation time by a factor of up to 4.8.

To our knowledge, no prior work has evolved GPU programs by directly handling the GPU machine code itself.

### 3. Quantum Computing and Quantum-Inspired Algorithms

In a classical computer, a *bit* is the smallest information unit and can take a value of 0 or 1. In a quantum computer, the basic information unit is the *quantum bit*, called the *qubit*. A qubit can take the states  $|0\rangle$  or  $|1\rangle$  or a superposition of the two. This superposition of the two states is a linear combination of the states  $|0\rangle$  and  $|1\rangle$  and can be represented as follows:

$$|\psi\rangle = \alpha |0\rangle + \beta |1\rangle, \quad (1)$$

where  $|\psi\rangle$  is the qubit state,  $\alpha$  and  $\beta$  are complex numbers, and  $|\alpha|^2$  and  $|\beta|^2$  are the probabilities that the qubit collapses to state 0 or 1, respectively, based on its observation (i.e., measurement). The unitary normalization guarantees the following:

$$|\alpha|^2 + |\beta|^2 = 1 \mid \{\alpha, \beta\} \in \mathbb{C}. \quad (2)$$

The superposition of states provides quantum computers with an incomparable degree of parallelism. This parallelism, when properly exploited, allows computers to perform tasks that are unfeasible in classical computers due to the prohibitive computational time.

Although quantum computing is promising in terms of processing capacity, there is still no technology for the actual implementation of a quantum computer, and there are only a few complex quantum algorithms.

Moore and Narayanan (1995) proposed a new approach to exploit the quantum computing concepts. Instead of developing new algorithms for quantum computers or attempting to make their use feasible, they proposed the idea of *quantum-inspired computing*. This new approach aims to create classical algorithms (i.e., running on classical computers) that utilize quantum mechanics paradigms to improve their problem-solving performance. In particular, quantum-inspired evolutionary algorithms (QEAs) have recently become a subject of special interest in evolutionary computation. The linear superposition of states represented in a qubit allows QEA to represent diverse individuals probabilistically. QEAs belong to the class of estimation of distribution algorithms (EDAs) (Platel et al., 2009). The probabilistic mechanism provides QEAs with an evolutionary mechanism that has several advantages, such as global search capability and faster convergence and smaller population size than those of traditional evolutionary algorithms. These algorithms have already been successfully used to solve various problems, such as the knapsack problem (Han and Kim, 2002), ordering combinatorial optimization problems (Silveira et al., 2012), engineering optimization problems (Alfares and Esat, 2006), image segmentation (Talbi et al., 2007), and image registration (Draa et al., 2004). See Zhang (2011) for more examples of QEAs and their applications.

#### 3.1 Multilevel Quantum Systems

Most quantum computing approaches use qubits encoded in two-level quantum systems. However, the candidate systems for encoding quantum information often have a more complex physical structure, with several directly accessible degrees of freedom (e.g., atoms, ions, photons). Quantum systems of  $d$  levels were recently studied, where the *qudit* is the quantum information unit, which may take any of  $d$  values or a superposition of  $d$  states (Lanyon et al., 2008).

## 4. Quantum-Inspired Linear Genetic Programming

The proposed quantum-inspired GP methodology for GPUs is based on the quantum-inspired linear genetic programming (QILGP) algorithm proposed by Dias and Pacheco (2013). QILGP evolves machine code programs for the Intel x86 platform. It uses floating point instructions and works with data from the main memory ( $m$ ) and/or eight FPU registers ( $ST(i) \mid i \in [0..7]$ ). The function set consists of addition, subtraction, multiplication, division, data transfer, trigonometric, and other arithmetic instructions. QILGP generates variable-sized programs by adding the NOP instruction to the instruction set. The code generation ignores any gene in which a NOP is present. Table 1 provides an example of a function set.

Each individual is represented by a linear sequence of machine code instructions. Each instruction can use one or zero arguments. The evaluation of a program requires the input data to be read from the main memory, which consists of the input variables of the problem and some optional constants supplied by the user. The input data are represented by a vector, such as

$$I = (V[0], V[1], 1, 2, 3), \quad (3)$$

where  $V[0]$  and  $V[1]$  have the two input values of the problem (i.e., a fitness case) and 1, 2, and 3 are the three constant values.

The instructions are represented in QILGP by two *tokens*: the *function token* (FT), which represents the function, and the *terminal token* (TT), which represents the argument of the function. Each function has a single terminal. When a function has no terminal, its corresponding token value is ignored. Each token is an integer value that represents an index to the function set or terminal set.

### 4.1 Representation

QILGP is based on the following entities: the *quantum individual*, which represents the superposition of all possible programs for the defined search space, and the *classical individual* (or *individual*), which represents the machine code program coded in the token values. A classical individual represents an individual of a traditional linear GP. In the observation phase of QILGP, each quantum individual is observed to generate one classical individual.

### 4.2 Observation

The chromosome of a quantum individual is represented by a list of structures called *quantum genes*. The observation of a quantum individual comprises the observations of all of its chromosome genes. The observation process consists of randomly generating a value  $r \in \mathbb{R} \mid 0 \leq r \leq 1$  and searching for the interval in which  $r$  belongs in all possible states that the individual can represent. For example, the process of observing a quantum gene

Instruction	Operation	Arg.
NOP	No operation	-
FADD $m$	$ST(\theta) \leftarrow ST(\theta) + m$	$m$
FADD ST(0), ST(i)	$ST(\theta) \leftarrow ST(\theta) + ST(i)$	$i$
FADD ST(i), ST(0)	$ST(i) \leftarrow ST(i) + ST(\theta)$	$i$
FSUB $m$	$ST(\theta) \leftarrow ST(\theta) - m$	$m$
FSUB ST(0), ST(i)	$ST(\theta) \leftarrow ST(\theta) - ST(i)$	$i$
FSUB ST(i), ST(0)	$ST(i) \leftarrow ST(i) - ST(\theta)$	$i$
FMUL $m$	$ST(\theta) \leftarrow ST(\theta) \times m$	$m$
FMUL ST(0), ST(i)	$ST(\theta) \leftarrow ST(\theta) \times ST(i)$	$i$
FMUL ST(i), ST(0)	$ST(i) \leftarrow ST(i) \times ST(\theta)$	$i$
FXCH ST(i)	$ST(\theta) \leftrightarrow ST(i)$ (swap)	$i$
FDIV $m$	$ST(\theta) \leftarrow ST(\theta) \div m$	$m$
FDIV ST(0), ST(i)	$ST(\theta) \leftarrow ST(\theta) \div ST(i)$	$i$
FDIV ST(i), ST(0)	$ST(i) \leftarrow ST(i) \div ST(\theta)$	$i$
FABS	$ST(\theta) \leftarrow  ST(\theta) $	-
FSQRT	$ST(\theta) \leftarrow \sqrt{ST(\theta)}$	-
FSIN	$ST(\theta) \leftarrow \sin ST(\theta)$	-
FCOS	$ST(\theta) \leftarrow \cos ST(\theta)$	-

Table 1: Functional description of the instructions. The first column presents the Intel x86 instructions. The second column presents the operations performed. The third column presents the argument of the instructions ( $m$  indexes memory positions, and  $i$  selects a register).

represented by 10 different states follows the function

$$T(r) = \begin{cases} 0 & \text{if } 0 \leq r < p'_0 \\ 1 & \text{if } p'_0 \leq r < p'_1 \\ 2 & \text{if } p'_1 \leq r < p'_2 \\ \vdots & \vdots \\ 9 & \text{if } p'_8 \leq r \leq p'_9, \end{cases} \quad (4)$$

where  $\{r \in \mathbb{R} \mid 0 \leq r \leq 1\}$  is the randomly generated value with a uniform distribution and  $T(r)$  returns the observed value for the token.

The observation process plays an important role in the quantum-inspired evolutionary algorithm. The quantum-inspired representation of a gene implies that the creation of each instruction follows a probabilistic distribution, where it is possible to represent the instructions that are more likely to be observed. Furthermore, the evolutionary algorithm can be fed with the results of the individual evaluations, and the superposition of states allows the probability values to be improved iteratively. The best classical individuals contribute to improving the probability values of the quantum individuals. This mechanism enables the algorithm to achieve better solutions with fewer evaluations.



0	1	2	3	-----
0.200	0.250	0.100	0.125	
$p_0$	$p_1$	$p_2$	$p_3$	

Figure 2: Illustration of a qudit implementation that represents Equation (6). Each state has an associated probability value and a token value. The observation process generates a random number  $r$  and selects one token based on the probability interval in which  $r$  fits.

QILGP is inspired by multilevel quantum systems (Lanyon et al., 2008), and uses the qudit as the basic information unit. This information can be described by a state vector of  $d$  levels, where  $d$  is the number of states in which the qudit can be measured. Accordingly,  $d$  represents the cardinality of the token. The state of a qudit is a linear superposition of  $d$  states and may be represented as follows:

$$|\psi\rangle = \sum_{i=0}^{d-1} \alpha_i |i\rangle, \tag{5}$$

where  $|\alpha_i|^2$  is the probability that the qudit collapses to state  $i$  when observed.

For example, suppose that each instruction in Table 1 has a unique token value in  $T = \{0,1,2,3,\dots\}$ . Equation (6) provides the state of a function qudit (FQ) whose state is given as follows:

$$|\psi\rangle = \frac{1}{\sqrt{5}} |0\rangle + \frac{1}{\sqrt{4}} |1\rangle + \frac{1}{\sqrt{10}} |2\rangle + \frac{1}{\sqrt{8}} |3\rangle + \dots \tag{6}$$

The probability of measuring the NOP instruction (state  $|0\rangle$ ) is  $(1/\sqrt{5})^2 = 0.200$ , for FADD  $m$  (state  $|1\rangle$ ) is  $(1/\sqrt{4})^2 = 0.250$ , for FADD ST(0),ST(i) (state  $|2\rangle$ ) is  $(1/\sqrt{10})^2 = 0.100$ , and so on. The qudit state of this example is implemented in a data structure as shown in Figure 2.

Figure 3 illustrates the creation of a classical gene by the observation of a quantum gene from an example based on Table 1 and the input vector  $I = (V[0], V[1], 1, 2, 3)$  (Equation 3). This process can be explained by three basic steps, indicated by the numbered circles in Figure 3:

1. The FQ is observed, and the resulting value (e.g., 7) is assigned to the FT of this gene.
2. The FT value determines the terminal qudit (TQ) to be observed, as each instruction requires a different type of terminal: register or memory.
3. The TQ defined by the FT value is observed, and the resulting value (e.g., 1) is assigned to the TT of this gene.

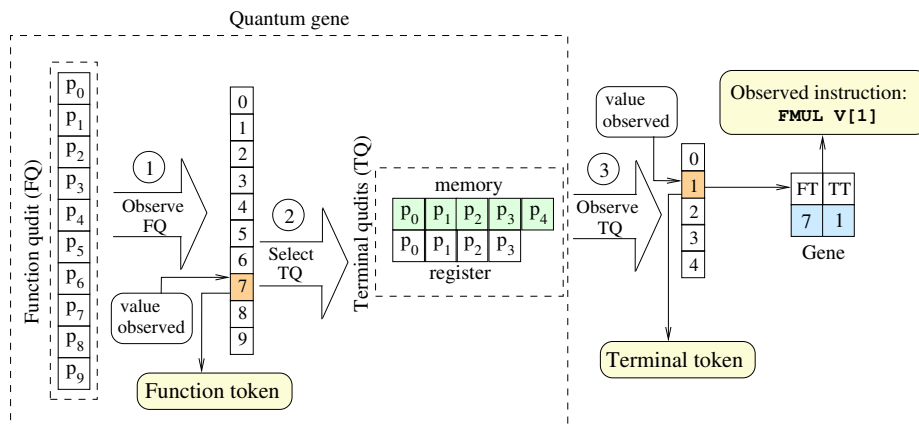


Figure 3: The creation of a classical gene from the observation of a quantum gene. The FQ is observed, and the token value selected is 7. The memory qudit is selected in the TQ. The TQ is observed, and the TT value selected is 1. The observed instruction in this example is `FMUL V[1]`, as ‘7’ is the FT value for this instruction (Table 1), and ‘1’ is the TT value that represents  $V[1]$  in the input vector  $I$  defined by Equation (3).

### 4.3 Evaluation of a Classical Individual

This process begins with the generation of a machine code program from the classical individual under evaluation, where its chromosome is sequentially traversed, gene by gene and token by token (both FTs and TTs), to serially generate the program body machine code related to the classical individual. Then, the program is executed for all fitness cases of the problem (i.e., samples of the training data set).

For each fitness case, the value assigned as the result of the fitness case is zero ( $V[0] \leftarrow 0$ ) when the instructions `FDIV` require division by zero or the instructions `FSQRT` require the calculation of the square root of a negative number.

### 4.4 Quantum Operator

The quantum operator of QILGP manipulates the probability  $p_i$  of a qudit, satisfying the normalization condition  $\sum_{i=0}^{d-1} |\alpha_i|^2 = 1$ , where  $d$  is the qudit cardinality and  $|\alpha_i|^2 = p_i$ . Operator  $P$  works in two main steps. First, it increases the given probability of a qudit as follows:

$$p_i \leftarrow p_i + s \times (1 - p_i), \tag{7}$$

where  $s$  is a parameter called *step size*, which can assume any real value between 0 and 1. The second step is to adjust the values of all of the probabilities of that qudit to satisfy the normalization condition. Thus, the operator modifies the state of a qudit by increasing  $p_i$  of a value that is directly proportional to  $s$ . The asymptotic behavior of  $p_i$  in Equation (7) indicates that the probability never reaches the unit value. This avoidance of unit probabilities is an important feature of this operator, as it avoids letting a probability

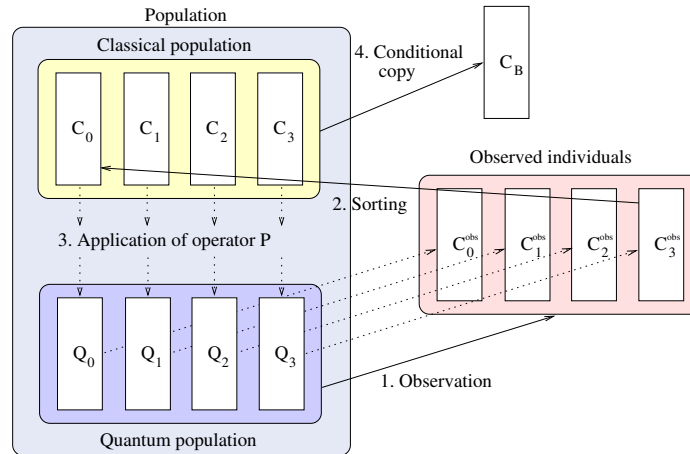


Figure 4: The four basic steps that characterize a generation of QILGP. With a population size of 4, the quantum individuals are observed and generate classical individuals. The classical individuals are sorted by their evaluations. The operator  $P$  is applied to each quantum individual, using the classical individual as the reference. The best classical individual evaluated thus far is kept in  $C_B$ .

cause the qudit to collapse, which could cause a premature convergence of the evolutionary search process.

QILGP has a hybrid population composed of a quantum population and classical population, both of which comprise  $M$  individuals. QILGP also has  $M$  auxiliary classical individuals  $C_i^{obs}$ , which result from observations of the quantum individuals  $Q_i$ , where  $1 \leq i \leq M$ .

#### 4.5 Evolutionary Algorithm

Figure 4 illustrates the four basic steps that characterize a *generation* of QILGP, with a population size  $M = 4$ . The algorithm works as follows:

1. Each of  $M$  quantum individuals is observed once, resulting in  $M$  classical individuals  $C_i^{obs}$ .
2. The individuals of the classical population and the observed individuals (auxiliary) are jointly sorted by their evaluations, ordered from best to worst, from  $C_0$  to  $C_{M-1}$ .
3. The operator  $P$  is applied to each quantum individual  $Q_i$ , taking their corresponding individual  $C_i$  in the classical population as a reference. Thus, at every new generation, the application of this operator increases the probability that the observations of the quantum individuals generate classical individuals more similar to the best individuals found thus far.
4. If any classical individual evaluated in the current generation is better than the best classical individual evaluated previously, a copy is stored in  $C_B$ , which keeps the best classical individual found by the algorithm thus far.

## 5. GPU Architecture

GPUs are highly parallel, many-core processors typically used as accelerators for a host system. They provide tremendous computational power and have proven to be successful for general-purpose parallel computing in a variety of application areas. Although different manufacturers have developed GPUs in recent years, we have opted for GPUs from Nvidia due to their flexibility and availability.

An Nvidia GPU consists of a set of streaming multiprocessors (SMs), each consisting of a set of GPU cores. The memory in the GPU is organized as follows: a large global memory with high latency; a very fast, low-latency on-chip shared memory for each SM; and a private local memory for each thread. Data communication between the GPU and CPU is conducted via the PCIe bus. The CPU and GPU have separate memory spaces, referred to as the host memory and device memory, and the GPU-CPU transfer time is limited by the speed of the PCIe bus.

### 5.1 Programming Model

The Nvidia programming model is CUDA (Computer Unified Device Architecture) (Nvidia, 2013). CUDA is a C-based development environment that allows the programmer to define special C functions, called *kernels*, which execute in parallel on the GPU by different threads. The GPU supports a large number of fine-grain threads. The threads are organized into a hierarchy of thread grouping. The threads are divided into a two- or three-dimensional *grid* of thread *blocks*. Each thread block is a two- or three-dimensional thread array. Thread blocks are executed on the GPU by assigning a number of blocks to be executed on a SM. Each thread in a thread block has a unique identifier, given by the built-in variables `threadIdx.x`, `threadIdx.y`, and `threadIdx.z`. Each thread block has an identifier that distinguishes its position in the grid, given by the built-in variables `blockIdx.x`, `blockIdx.y`, and `blockIdx.z`. The dimensions of the thread and thread block are specified at the time when the kernel is launched through the identifiers `blockDim` and `gridDim`, respectively.

All threads in a block are assigned to execute in the same SM. Hence, threads within one block can cooperate among themselves using synchronization primitives and shared memory. However, the number of threads within one block can exceed the number of cores in an SM, which requires a scheduling mechanism. The scheduling mechanism divides the block into *warps*. Each warp contains a fixed number of threads grouped by consecutive thread identifiers. The warp is executed on an SM in an implicit SIMD fashion, called SIMT (single instruction, multiple threads). Each core of an SM executes the same instruction simultaneously but on different data elements. However, the threads may logically follow a different control flow path and are free to branch. If some of the parallel threads choose a different execution path, called *code divergence*, their execution is serialized. In this case, the warp must be issued multiple times, one for each group of divergent threads. Thus, full efficiency is accomplished only when all of the threads in the warp follow the same execution path; otherwise, parallel efficiency can degrade significantly.

## 5.2 Compilation

The compilation of a CUDA program is performed through the following stages. First, the CUDA front end, *cudafe*, divides the program into the C/C++ host code and GPU device code. The host code is compiled with a regular C compiler, such as *gcc*. The device code is compiled using the CUDA compiler, *nvcc*, generating an intermediate code in an assembly language called PTX (Parallel Thread Execution). PTX is a human-readable, assembly-like low-level programming language for Nvidia GPUs that is compiled and hides many of the machine details. PTX has been fully documented by Nvidia. The PTX code is then translated to the GPU binary code, CUBIN, using the *ptxas* compiler.

Unlike the PTX language, whose documentation has been made public, the CUBIN format is proprietary, and no information has been made available by Nvidia. All of the work performed with CUBIN requires reverse engineering. In addition, the manufacturer provides only the most basic elements of the underlying hardware architecture, and there are apparently no plans to make more information public in the future.

## 6. GPU Machine Code Genetic Programming

Our GP methodology for GPUs is called GPU Machine Code Genetic Programming **GMGP**. It is a quantum-inspired LGP, based on QILGP, that evaluates the individuals on the GPU. The concept is to exploit the probabilistic representation of the individuals to achieve fast convergence and to parallelize the evaluation using the GPU machine code directly.

Before the evolution begins, the entire data set is transferred to the GPU global memory. In the first step, all of the classical individuals of one generation are created in the CPU in the same manner as in QILGP. Each classical individual is composed of tokens representing the instructions and arguments. For each individual, GMGP creates a GPU machine code kernel. These programs are then loaded to the GPU program memory and executed in parallel. The evaluation process in GMGP is performed with a high level of parallelism. We exploit the parallelism as follows: individuals are processed in parallel in different thread blocks, and data parallelism is exploited within each thread block, where each thread evaluates a different fitness case.

When the number of fitness cases is smaller than the number of threads in the block, we map one individual per block. For fitness cases greater than the number of threads per block, a two-dimensional grid is used, and each individual is mapped on multiple blocks. The individual is identified by the `blockIdx.y`, and the fitness case is identified by `(blockIdx.x * blockDim.x + threadIdx.x)`. To maintain all of the individual codes in a single GPU kernel, we use a set of IF statements to distinguish each individual. However, these IF statements do not introduce divergence in the kernel because all of the threads in each block follow the same execution path.

This methodology allows for the rapid evaluation of individuals. The GPU binary code is directly modified, thus avoiding the need to compile individuals. Regarding the machine code, our implementation is based on the Nvidia CUBIN code for the current Nvidia GPU architectures. Future Nvidia GPU machine code could be evolved using our methodology as long as the opcodes are known.

## 6.1 Function Set

GMGP is capable of evolving linear sequences of single precision floating point operations or linear sequences of Boolean operations. The function set of floating point operations is composed of addition, subtraction, multiplication, division, data transfer, trigonometric, and arithmetic instructions. The function set of Boolean operations is composed of AND, OR, NAND, NOR, and NOT. Table 2 provides the instruction set of the floating point operations, and Table 3 provides the instruction set of the Boolean operations. Each of these instructions has an opcode and one or two arguments. The argument can be a register or memory position. When it is a register, it varies from  $R0$  to  $R7$ . When it is a memory position, it can be used to load input data or a constant value. The maximum number of inputs in GMGP is 256, and the maximum number of predefined constant values is 128. As an example, in Table 4, we present the CUBIN add instruction with all of the variations of its memory positions ( $X$ ) and the eight auxiliary FPU registers ( $Ri \mid i \in [0..7]$ ). Each CUBIN instruction variation with its arguments (constants or registers) has a different hexadecimal.

GMGP addresses only floating point and Boolean operations. Loops and jumps are not handled, as they are not common in the benchmark problems that we consider. However, GMGP could be extended to consider such problems, including mechanisms to restrict jumping to invalid positions and to avoid infinite loops.

Each evolved CUBIN program consists of three segments: *header*, *body*, and *footer*. The header and footer are the same for all individuals throughout the evolutionary process. They are optimized in the same manner as by the Nvidia compiler. These segments contain the following:

- *Header* – Loads the evaluation patterns from global memory to registers on the GPU and initializes eight registers with zero.
- *Body* – The evolved CUBIN code itself.
- *Footer* – Transfers  $R0$  contents to the global memory, which is the default output of evolved programs, and then executes the exit instruction to terminate the program and return to the evolutionary algorithm main flow.

For each individual, the body of the program is assembled by stacking the hexadecimal code in the same order as the GP tokens have been read. There is no need for comparisons and branches within an individual code because the instructions are executed sequentially. Avoiding comparisons and branches is an important feature of GMGP. As explained before, GPUs are particularly sensitive to conditional branches.

We aggregate all program bodies of the same population into a single GPU kernel. The kernel has only one header and one footer, reducing the size of the population and thus decreasing the time to transfer the program to the GPU memory through the PCIe bus.

## 6.2 Machine Code Acquisition

We developed a semi-automatic procedure to acquire the GPU machine code instructions. Nvidia does not provide any documentation for its machine code.

CUDA	PTX	Description	A
		No operation	-
R0+=Xj ;	add.f32 R0, R0, Xj ;	$R(0) \leftarrow R(0) + X(j)$	$j$
R0+=Ri ;	add.f32 R0, R0, Ri ;	$R(0) \leftarrow R(0) + R(i)$	$i$
Ri+=R0 ;	add.f32 Ri, Ri, R0 ;	$R(i) \leftarrow R(i) + R(0)$	$i$
R0-=Xj ;	sub.f32 R0, R0, Xj ;	$R(0) \leftarrow R(0) - X(j)$	$j$
R0-=Ri ;	sub.f32 R0, R0, Ri ;	$R(0) \leftarrow R(0) - R(i)$	$i$
Ri-=R0 ;	sub.f32 Ri, Ri, R0 ;	$R(i) \leftarrow R(i) - R(0)$	$i$
R0*=Xj ;	mul.f32 R0, R0, Xj ;	$R(0) \leftarrow R(0) \times X(j)$	$j$
R0*=Ri ;	mul.f32 R0, R0, Ri ;	$R(0) \leftarrow R(0) \times R(i)$	$i$
Ri*=R0 ;	mul.f32 Ri, Ri, R0 ;	$R(i) \leftarrow R(i) \times R(0)$	$i$
R0/=Xj ;	div.full.f32 R0, R0, Xj ;	$R(0) \leftarrow R(0) \div X(j)$	$j$
R0/=Ri ;	div.full.f32 R0, R0, Ri ;	$R(0) \leftarrow R(0) \div R(i)$	$i$
Ri/=R0 ;	div.full.f32 Ri, Ri, R0 ;	$R(i) \leftarrow R(i) \div R(0)$	$i$
R8=R0;R0=Ri;Ri=R8;	mov.f32 R8, R0 ; mov.f32 R0, Ri ; mov.f32 Ri, R8 ;	$R(0) \xleftrightarrow{\leftarrow} R(i)$ (swap)	$i$
R0=abs(R0) ;	abs.f32 R0, R0 ;	$R(0) \leftarrow  R(0) $	-
R0=sqrt(R0) ;	sqrt.approx.f32 R0, R0 ;	$R(0) \leftarrow \sqrt{R(0)}$	-
R0=__sinf(R0) ;	sin.approx.f32 R0, R0 ;	$R(0) \leftarrow \sin R(0)$	-
R0=__cosf(R0) ;	cos.approx.f32 R0, R0 ;	$R(0) \leftarrow \cos R(0)$	-

Table 2: Functional description of the single precision floating point instructions. The first column presents the CUDA command; the second presents the PTX instruction; the third describes the action performed; and the fourth column presents the argument for the instruction ( $j$  indexes memory positions, and  $i$  selects a register). The last two instructions, `__sinf` and `__cosf`, are `fast_math` instructions, which are less accurate but faster versions of `sinf` and `cosf`.

Our procedure creates a PTX program containing all of the PTX instructions listed in Tables 2 or 3. In this program, each instruction is embodied inside a loop, where the iteration count at the start of the loop is unknown, which prevents the `ptxas` compiler from removing instructions.

The PTX program is compiled, and the Nvidia `cuobjdump` tool is used to disassemble the binary code. The disassembled code contains the machine code of all instructions of the PTX program. The challenge is to remove the instructions that belong to each loop control, which is achieved by finding a pattern that repeats along the code. Once the loop controls are removed, each instruction of our instruction set is acquired.

The header and footer are obtained using the `xxd` tool from Linux, which converts binary programs into hex code and transforms the entire program into hexadecimal representation.

CUDA	PTX	Description	A
		No operation	-
$R0=R0 \ \& \ Xj$ ;	and.b32 R0, R0, Xj ;	$R(0) \leftarrow R(0) \wedge X(j)$	$j$
$R0=R0 \ \& \ Ri$ ;	and.b32 R0, R0, Ri ;	$R(0) \leftarrow R(0) \wedge R(i)$	$i$
$Ri=Ri \ \& \ R0$ ;	and.b32 Ri, Ri, R0 ;	$R(i) \leftarrow R(i) \wedge R(0)$	$i$
$R0=R0 \ \text{---} \ Xj$ ;	or.b32 R0, R0, Xj ;	$R(0) \leftarrow R(0) \vee X(j)$	$j$
$R0=R0 \ \text{---} \ Ri$ ;	or.b32 R0, R0, Ri ;	$R(0) \leftarrow R(0) \vee R(i)$	$i$
$Ri=Ri \ \text{---} \ R0$ ;	or.b32 Ri, Ri, R0 ;	$R(i) \leftarrow R(i) \vee R(0)$	$i$
$R0= \sim (R0 \ \& \ Xj)$ ;	and.b32 R0, R0, Xj ; not.b32 R0, R0 ;	$R(0) \leftarrow \overline{R(0) \wedge X(j)}$	$j$
$R0= \sim (R0 \ \& \ Ri)$ ;	and.b32 R0, R0, Ri ; not.b32 R0, R0 ;	$R(0) \leftarrow \overline{R(0) \wedge R(i)}$	$i$
$Ri= \sim (Ri \ \& \ R0)$ ;	and.b32 Ri, Ri, R0 ; not.b32 Ri, Ri ;	$R(i) \leftarrow \overline{R(i) \wedge R(0)}$	$i$
$R0= \sim (R0 \ \text{---} \ Xj)$ ;	or.b32 R0, R0, Xj ; not.b32 R0, R0 ;	$R(0) \leftarrow \overline{R(0) \vee X(j)}$	$j$
$R0= \sim (R0 \ \text{---} \ Ri)$ ;	or.b32 R0, R0, Ri ; not.b32 R0, R0 ;	$R(0) \leftarrow \overline{R(0) \vee R(i)}$	$i$
$Ri= \sim (Ri \ \text{---} \ R0)$ ;	or.b32 Ri, Ri, R0 ; not.b32 Ri, Ri ;	$R(i) \leftarrow \overline{R(i) \vee R(0)}$	$i$
$R0= \sim R0$ ;	not.b32 R0, R0 ;	$R(0) \leftarrow \overline{R(0)}$	-

Table 3: Functional description of the Boolean instructions. The first column presents the CUDA command; the second presents the PTX instruction; the third describes the action performed; and the fourth column presents the argument for the instruction ( $j$  indexes memory positions, and  $i$  selects a register).

The header is the code that comes before the first instruction found, and the footer is the remaining code after the last instruction found.

With the header and footer, our procedure generates a different program to test each instruction acquired. This program contains a header, a footer, and one instruction. The program is executed, and the result is compared to an expected result that was previously computed on the CPU.

### 6.3 Evaluation Process

The GMGP methodology was explicitly designed to exploit the highly parallel capabilities of the GPU architecture. Because GMGP evaluates the entire population at once using two levels of parallelism, i.e., at the individual level and at the fitness case level, we expect our methodology to readily exploit future GPU architectures that are likely to have more processing cores than the recent releases. GMGP utilizes the independence of the fitness case execution and the ability to evaluate the individuals in parallel. In addition, this



CUBIN (hexadecimal representation)	Description	A
<b>0x7e</b> , 0x7c, 0x1c, <b>0x9</b> , 0x0, <b>0x80</b> , 0xc0, <b>0xe2</b> , <b>0x7e</b> , 0x7c, 0x1c, <b>0xa</b> , 0x0, <b>0x80</b> , 0xc0, <b>0xe2</b> , 0x7d, 0x7c, 0x1c, 0x0, <b>0xfc</b> , <b>0x81</b> , 0xc0, 0xc2, 0x7d, 0x7c, 0x1c, 0x0, <b>0x0</b> , 0x82, 0xc0, 0xc2, 0x7d, 0x7c, 0x1c, 0x0, <b>0x2</b> , 0x82, 0xc0, 0xc2, 0x7d, 0x7c, 0x1c, 0x0, <b>0x4</b> , 0x82, 0xc0, 0xc2, 0x7d, 0x7c, 0x1c, 0x0, <b>0x5</b> , 0x82, 0xc0, 0xc2, 0x7d, 0x7c, 0x1c, 0x0, <b>0x6</b> , 0x82, 0xc0, 0xc2, 0x7d, 0x7c, 0x1c, 0x0, <b>0x7</b> , 0x82, 0xc0, 0xc2, 0x7d, 0x7c, 0x1c, 0x0, <b>0x8</b> , 0x82, 0xc0, 0xc2, 0x7d, 0x7c, 0x1c, <b>0x80</b> , <b>0x8</b> , 0x82, 0xc0, 0xc2,	$R(0) \leftarrow R(0) + X(j)$	<i>j</i>
0x7e, 0x7c, <b>0x9c</b> , <b>0x0f</b> , 0x0, 0x80, 0xc0, 0xe2, 0x7e, 0x7c, <b>0x1c</b> , <b>0x0</b> , 0x0, 0x80, 0xc0, 0xe2, 0x7e, 0x7c, <b>0x1c</b> , <b>0x3</b> , 0x0, 0x80, 0xc0, 0xe2, 0x7e, 0x7c, <b>0x9c</b> , <b>0x3</b> , 0x0, 0x80, 0xc0, 0xe2, 0x7e, 0x7c, <b>0x1c</b> , <b>0x4</b> , 0x0, 0x80, 0xc0, 0xe2, 0x7e, 0x7c, <b>0x9c</b> , <b>0x4</b> , 0x0, 0x80, 0xc0, 0xe2, 0x7e, 0x7c, <b>0x1c</b> , <b>0x5</b> , 0x0, 0x80, 0xc0, 0xe2, 0x7e, 0x7c, <b>0x9c</b> , <b>0x5</b> , 0x0, 0x80, 0xc0, 0xe2,	$R(0) \leftarrow R(0) + R(i)$	<i>i</i>
<b>0x7e</b> , 0x7c, <b>0x9c</b> , <b>0x0f</b> , 0x0, 0x80, 0xc0, 0xe2, <b>0x2</b> , 0x7c, <b>0x1c</b> , <b>0x0</b> , 0x0, 0x80, 0xc0, 0xe2, <b>0x1a</b> , 0x7c, <b>0x1c</b> , <b>0x3</b> , 0x0, 0x80, 0xc0, 0xe2, <b>0x1e</b> , 0x7c, <b>0x9c</b> , <b>0x3</b> , 0x0, 0x80, 0xc0, 0xe2, <b>0x22</b> , 0x7c, <b>0x1c</b> , <b>0x4</b> , 0x0, 0x80, 0xc0, 0xe2, <b>0x26</b> , 0x7c, <b>0x9c</b> , <b>0x4</b> , 0x0, 0x80, 0xc0, 0xe2, <b>0x2a</b> , 0x7c, <b>0x1c</b> , <b>0x5</b> , 0x0, 0x80, 0xc0, 0xe2, <b>0x2e</b> , 0x7c, <b>0x9c</b> , <b>0x5</b> , 0x0, 0x80, 0xc0, 0xe2,	$R(i) \leftarrow R(i) + R(0)$	<i>i</i>

Table 4: Hexadecimal representation of the add GPU machine code instruction.

parallelization scheme avoids code divergence, as each thread in a block executes the same instruction over a different fitness case, and different individuals are executed by different thread blocks. Therefore, we are employing as much parallelism as possible for a population.

The evaluation process addresses the problems caused by execution errors, such as divisions by zero or square roots of negative numbers, which directly affect the fitness value of an evolved program. In both cases, the value assigned as the result is zero ( $Ri \leftarrow 0$ ), which is the same approach adopted by the QILGP implementation (Dias and Pacheco, 2009).

## 7. Experiments and Results

In this section, we analyze the performance of GMGP compared with the other GP methodologies for GPUs. We describe the environment setup, the implementation of the other GP methodologies, the benchmarks, and the analysis of the results obtained from our experiments.

### 7.1 Environment Setup

The GPU used in our experiments was the GeForce GTX TITAN. This processor has 2,688 CUDA cores (at 837 MHz) and 6 GB of RAM (no ECC) with a memory bandwidth of 288.4 GB/s through a 384-bit data bus. The GTX TITAN GPU is based on the Nvidia Kepler architecture, and its theoretical peak performance is characterized by the use of the fused multiply-add (FMA) operations. The GTX TITAN can achieve single precision theoretical peak performance of 4.5 TFLOPs.

GMGP creates the individuals on CPU using a single-threaded code running on a single core of an Intel Xeon CPU X5690 processor, with 32 KB of L1 data cache, 1.5 M of L2 cache, 12 MB of L3 cache, and 24 GB of RAM, running at 3.46 GHz.

The GP methodologies were implemented in C, CUDA 5.5, and PTX 3.2. The compilers used were gcc 4.4.7, nvcc release 5.5, V5.5.0, and ptxas release 5.5, V5.5.0. We had to be careful in setting the compiler optimization level. It is common for the programmer to use a more advanced optimization level to produce a more optimized and faster code. However, the compilation time is a bottleneck for the GP methodologies that require individuals to be compiled. The code generated by the -O2, -O3, and -O4 optimization levels is more optimized and executes faster, but more time is spent in the compilation process. Experiments were performed to determine the best optimization level. These experiments indicated that the lowest optimization level, -O0, provided the best results. There were millions of individuals to be compiled, and each individual was executed only once. Accelerating the execution phase was not sufficient to compensate for the time spent optimizing the code during the compilation phase.

We used five widely used GP benchmarks: two symbolic regression problems, *Mexican Hat* and *Salutowicz*; one time-series forecasting problem, *Mackey-Glass*; one image processing problem, *Sobel filter*; and one Boolean regression problem, *20-bit Multiplexer*. The first four benchmarks were used to evaluate the single precision floating point instructions, whereas the last benchmark was used to evaluate the Boolean instructions. The *Mackey-Glass*, *Boolean Multiplexer*, and *Sobel filter* benchmarks were also used in previous works on GP accelerated by GPUs (Robilliard et al., 2009; Langdon and Banzhaf, 2008c; Langdon, 2010b; Harding and Banzhaf, 2008, 2009). Nevertheless, it is not possible to perform a direct comparison, as they used a different GP model (tree-based GP) and different hardware.

Each result in the experiments was obtained by repeating the experiment 10 times and averaging the timing results. The standard deviations of the times obtained for all the data sets were less than 5% of the average execution times. We present our timing results in both seconds and GP operations per second (GPOps), which has been widely used in previous GP works. Although the focus of the paper is on the actual execution speeds of the GP evaluation, we briefly discuss the quality of the results produced by GMGP and the other methodologies studied.

We used 256 threads per block in our experiments. The block grid is two-dimensional and depends on the number of individuals and the number of fitness cases. For an experiment with  $(number\_fitness\ cases, number\_individuals)$  the grid is  $(number\_fitness\ cases/256, number\_individuals)$ .

## 7.2 GP Implementations

To put the GMGP results in perspective, we compare the performance of GMGP with the other GP methodologies for GPUs: *compilation*, *pseudo-assembly*, and *interpretation*. However, the GP methodologies for GPUs taken from the literature are not based on LGP or quantum-inspired algorithms. For this reason, we had to implement an LGP and quantum-inspired approach corresponding to each methodology to make them directly comparable with GMGP. Nevertheless, these implementations are based on the algorithms described in the literature.

The *compilation* approach is based on the work by Harding and Banzhaf (2009) and is called **Compiler** here. The *pseudo-assembly* approach is based on our previous work (Cupertino et al., 2011), and is called **Pseudo-Assembly** here. The *interpretation* approach is based on the work by Langdon and Banzhaf (2008a) and is called **Interpreter** here.

The Compiler and Pseudo-Assembly methodologies use a similar program assembly to the GMGP methodology. The individuals are created by the CPU and sent to the GPU to be computed. The main difference is the assembly of the body of the programs. In Compiler, the bodies are created using CUDA language instructions. When the population is complete, it is compiled using the *nvcc* compiler to generate the GPU binary code. In Pseudo-Assembly, the bodies are created using the PTX pseudo-assembly language instructions. When the population is complete, the code can be compiled with *ptxas* or the *cuModuleLoadC* function provided by Nvidia, both of which generate GPU binary code. The Pseudo-Assembly methodology reduces the compilation overhead using the JIT compilation.

In the Interpreter methodology, the interpreter was written in the PTX language, rather than in RapidMind, as proposed by Langdon and Banzhaf (2008a). The interpreter is automatically built once, at the beginning of the GP evolution, and is reused to evaluate all individuals. Algorithm 1 presents a high-level description of the interpreter process. As the pseudo-assembly language does not have a switch-case statement, we used a combination of the instruction `setp.eq.s32` (comparisons) and `bra` (branches) to obtain the same functionality. These comparisons and branches represent one of the weaknesses of the Interpreter methodology. The interpreter must execute more instructions than the actual GP operations. For each GP instruction, we have at least one comparison, to identify the GP operation, and one jump to the beginning of the loop. In addition, comparisons can be made to identify the instruction arguments.

The GP methodologies implemented employ an equivalent function set and use the same number of registers. In QILGP (Dias and Pacheco, 2013), the function set has an atomic exchange instruction (`FXCH ST(i)`) that the GPU does not have. To maintain the function set compatibility with QILGP in the experiments, we created the exchange operation in the GPU using three move operations. An exchange between  $R_i$  and  $R_0$  uses an intermediary register  $R_8$  and becomes  $R_8 = R_0$ ;  $R_0 = R_i$ ;  $R_i = R_8$ , as shown in Table 2.

```

1:  $TBX \leftarrow$  X dimension of the Thread Block identification
2:  $TBY \leftarrow$  Y dimension of the Thread Block identification
3:  $INDIV \leftarrow$  individual number ( $TBY$ )
4:  $N \leftarrow$  program length ( $INDIV$ )
5:  $THREAD \leftarrow$  GPU Thread identification
6:  $X0 \leftarrow$  input variable 1 ( $THREAD + TBX * \text{Number of threads in a block}$ )
7:  $X1 \leftarrow$  input variable 2 ( $THREAD + TBX * \text{Number of threads in a block}$ )
8: for  $k \leftarrow 1$  to  $N$  do
9:    $INSTRUCT \leftarrow$  instruction number ( $k$ ) ( $INDIV$ )
10:   $ARG \leftarrow$  argument number ( $k$ ) ( $INDIV$ )
11:  switch ( $INSTRUCT$ )
12:  case 0:
13:    no operation
14:  case 1:
15:    switch ( $ARG$ )                                % Description:  $R(0) \leftarrow R(0) + X(j)$ 
16:    case 0:
17:      add.f32 R0, R0, X0
18:    case 1:
19:      add.f32 R0, R0, X1
20:     $\rightarrow$  Here, we have more similar cases for all inputs and constant registers ( $X$ ).
21:    end switch
22:  case 2:
23:    switch ( $ARG$ )                                % Description:  $R(0) \leftarrow R(0) + R(i)$ 
24:    case 0:
25:      add.f32 R0, R0, R0
26:    case 1:
27:      add.f32 R0, R0, R1
28:     $\rightarrow$  Here, we have more similar cases for all eight auxiliary FPU registers ( $R_i$ ).
29:    end switch
30:  case 3:
31:    switch ( $ARG$ )                                % Description:  $R(i) \leftarrow R(i) + R(0)$ 
32:    case 0:
33:      add.f32 Ri, R0, R0
34:    case 1:
35:      add.f32 Ri, R1, R0
36:     $\rightarrow$  Here, we have more similar cases for all eight auxiliary FPU registers ( $R_i$ ).
37:    end switch
38:     $\rightarrow$  Here, we have more similar cases for all other instructions, such as subtraction, multiplication,
    division, data transfer, trigonometric, and arithmetic operations.
39:  default:
40:    exit
41:  end switch
42:   $\rightarrow$  Write result back to global memory.
43: end for

```

**Algorithm 1:** Pseudo-code for the GP interpreter for a GPU based on quantum-inspired LGP.

### 7.3 Symbolic Regression Benchmarks

Symbolic regression is a typical problem used to assess GP performance. We used two well-known benchmarks: the *Mexican Hat* and *Salutowicz*. These benchmarks allow us to evaluate GMGP over different fitness case sizes.

The *Mexican Hat* benchmark (Brameier and Banzhaf, 2007) is represented by a two-dimensional function given by Equation (8):

$$f(x,y) = \left(1 - \frac{x^2}{4} - \frac{y^2}{4}\right) \times e^{(-x^2-y^2)/8}. \quad (8)$$

The *Salutowicz* benchmark (Vladislavleva et al., 2009) is represented by Equation (9). We used the two-dimensional version of this benchmark.

$$f(x,y) = (y - 5) \times e^{-x} \times x^3 \times \cos(x) \times \sin(x) \times \left[\cos(x) \times \sin(x)^2 - 1\right]. \quad (9)$$

For the *Mexican Hat* benchmark, the  $x$  and  $y$  variables are uniformly sampled in the range  $[-4,4]$ . For the *Salutowicz* benchmark, they are uniformly sampled in the range  $[0,10]$ . This sampling generates the training, validation, and testing data sets. The number of subdivisions of each variable can be 16, 32, 64, 128, 256, and 512, which is called the number of samples,  $N$ . At each time, both variables use the same value of  $N$ , producing a grid. When  $N = 16$ , there is a  $16 \times 16$  grid, which represents 256 fitness cases. Accordingly, the number of fitness cases varies in the set  $S = \{256, 1024, 4096, 16K, 64K, 256K\}$ .

These two benchmarks represent two different surfaces, and GP has the task of reconstructing these surfaces from a given set of points. The fitness value of an individual is its mean absolute error (MAE) over the training cases, as given by Equation (10):

$$\text{MAE} = \frac{1}{n} \sum_{i=1}^n |t_i - V[0]_i|, \quad (10)$$

where  $t_i$  is the target value for the  $i$ th case and  $V[0]_i$  is the individual output value for the same case.

#### 7.3.1 PARAMETER SETTINGS

Table 5 presents the parameters used when executing the *Mexican Hat* and *Salutowicz* benchmarks. We used a small population size, which is a typical characteristic of QEAs. The evolution status of QEAs is represented by a probability distribution, and there is no need to include many individuals. The superposition of states provides a good global search ability due to the diversity provided by the probabilistic representation.

#### 7.3.2 PRELIMINARY EXPERIMENTS FOR THE COMPILER METHODOLOGY

Table 6 presents the execution time breakdown of all GPU methodologies for the *Mexican Hat* benchmark when the fitness case is 16K. The execution time is broken down into the following categories: `nvcc` represents the time spent with the `nvcc` compiler to generate the PTX code from the CUDA source code; `upload` represents the time spent compiling the PTX code to the GPU binary code (in our methodology, `upload` means the time spent loading

Parameter	Settings	
	Mexican Hat	Salutowicz
Number of generations	400,000	400,000
Population size	36	36
NOP initial probability ( $\alpha_{0,0}$ )	0.9	0.9
Step size ( $s$ )	0.0003	0.002
Maximum program length	128	128
Function set	Table 2	Table 2
Set of constants	{1,2,3,4,5,6,7,8,9}	{1,2,3,4,5,6,7,8,9}

Table 5: Parameter settings for the Mexican Hat and Salutowicz benchmarks. The values of number of generations, population size, initial probability of NOP, and step size were obtained from previous experiments.

Methodology	Total	nvcc	upload	evaluation	interpret	download	CPU
GMGP	292.6	–	73.2	76.9	–	5.13	137.2
Interpreter	636.8	–	3.14	–	542.4	4.35	86.8
Pseudo-Assembly	40,777	–	40,414	118.8	–	6.13	238.8
Compiler	242,186.7	135,027.5	106,458	283.6	–	6.74	410.9

Table 6: Execution time breakdown of all GPU methodologies (in seconds). The table presents the times for: **Total**, the total execution; **nvcc**, the compilation in the *nvcc* compiler; **upload**, the compilation of the PTX code (Compiler and Pseudo-Assembly), or loading the GPU binaries to the GPU memory (GMGP), or transferring the tokens through the PCIe bus (Interpreter); **evaluation**, the computation of the fitness cases; **interpret**, the interpretation; **download**, the copy of the fitness result from GPU to the CPU; and **CPU**, the GP methodology is executed on the CPU.

the GPU binaries to the graphic card before execution); in the interpreter methodology, **upload** is the time necessary to transfer the tokens through the PCIe bus; **evaluation** represents the time spent computing the fitness cases; **interpret** is the interpretation time for Interpreter; **download** is the time spent in copying the fitness result from GPU to the CPU; and **CPU** represents the remainder of the execution time, including the time necessary to execute the GP methodology on the CPU.

As can be observed in Table 6, the Compiler methodology is the only one that spends time on the *nvcc* compiler. The time spent on the *nvcc* compiler is enormous when compared to all other times, and Compiler becomes three orders of magnitude slower than GMGP and Interpreter. Although some previous works have reported results for the Compiler methodology for GP in GPUs (Harding and Banzhaf, 2007; Chitty, 2007; Harding and Banzhaf, 2009; Langdon and Harman, 2010), they are not comparable with our results. Harding and

Banzhaf (2007) and Chitty (2007) did not use CUDA and could therefore avoid the *nvcc* overhead. Harding and Banzhaf (2009) used CUDA but handled the compilation overhead by using a cluster to compile the population. Langdon and Harman (2010) also used CUDA, but the total compilation time for our experiment is greater than their compilation time for two reasons. First, the small population size of a quantum-inspired approach requires more compiler calls. Second, the total number of individuals we are evaluating (number of generations  $\times$  population size) is at least one order of magnitude greater than in their experiments.

Because the other methodologies solved the same problem considerably faster, we discarded the Compiler methodology for the remaining experiments.

The `download` time is almost the same for all implementations because the same data set was used in all approaches. Accordingly, the results to be copied through the PCIe bus are the same. The `CPU` time for Interpreter is slightly smaller than for GMGP, Compiler, and Pseudo-Assembly because Interpreter does not have to assemble the individuals in the CPU before transferring to the GPU. Instead, the tokens are copied directly. The `evaluation` time is almost the same for Compiler and Pseudo-Assembly, but GMGP presents a slightly smaller `evaluation` time because the header and footer are optimized. The `interpret` time is approximately one order of magnitude slower than the GMGP `evaluation` time because it has to perform many additional instructions, such as comparisons and jumps. The `upload` time for GMGP is approximately three orders of magnitude faster than the `upload` time for Compiler and Pseudo-Assembly because GMGP directly assembles the GPU binaries without calling the PTX compiler. The time necessary to transfer the tokens through the PCIe bus in the Interpreter methodology is smaller than the time necessary to load the GPU binary code in the GMGP.

### 7.3.3 PERFORMANCE ANALYSIS

We compare the execution times of the methodologies as the number of fitness cases varies in the set:  $S = \{256, 1024, 4096, 16K, 64K, 256K\}$ . The total execution times of the *Mexican Hat* and *Salutowicz* benchmarks for the Pseudo-Assembly, Interpreter, and GMGP methodologies are presented in Figure 5. The curves are plotted in log-scale. The Pseudo-Assembly methodology execution time remains almost constant as the problem size increases in both cases studied because Pseudo-Assembly spends most of the time compiling the individual population code, and the compilation time does not depend on the problem size. The total execution times of the Interpreter and GMGP methodologies increase almost linearly as the number of fitness cases increases from 256 to 256K. For the largest data set, 256K, the Pseudo-Assembly execution time approaches the execution time of Interpreter. However, the Pseudo-Assembly methodology performs much worse than the other methodologies when only a few fitness cases are considered.

In Table 7, we present the performance of the three methodologies for a 256K data set, using the GP operations per second (GPops) metric, which is widely employed in the GP literature. Considering the total evolution, GMGP performs  $2.29e+014$  GP operations on  $1.17e+003$  seconds, obtaining 194.4 billion GPops for *Mexican Hat*. Similarly, GMGP obtained 200.5 billion GPops for *Salutowicz*. The Interpreter methodology took 26.6 billion GPops for *Mexican Hat* and 27.5 billion GPops for *Salutowicz*. The Pseudo-Assembly

Benchmark	Methodology	GP evolution (GPops)	Best Individual (GPops)
Mexican Hat	GMGP	194.4 billion	245.5 billion
	Interpreter	26.6 billion	29.9 billion
	Pseudo-Assembly	5.3 billion	161.0 billion
Salutowicz	GMGP	200.5 billion	240.2 billion
	Interpreter	27.5 billion	27.0 billion
	Pseudo-Assembly	4.9 billion	158.4 billion

Table 7: Performance of GMGP, Interpreter, and Pseudo-Assembly for *Mexican Hat* and *Salutowicz* in GPops. The table presents the results for the overall evolution, including the time spent in the GPU and CPU, and the results for the GPU computation of the best individual after the evolution is complete.

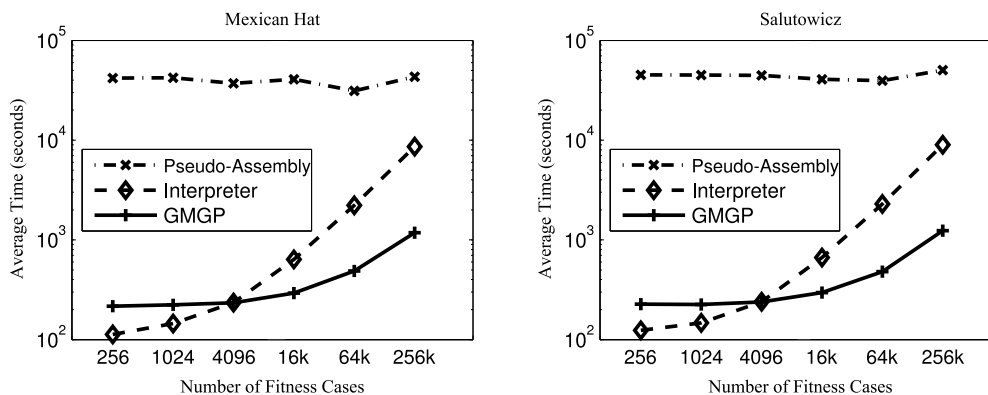


Figure 5: Execution time (in seconds) of Pseudo-Assembly, Interpreter, and GMGP methodologies for the *Mexican Hat* and *Salutowicz* benchmarks with an increasing number of fitness cases.

methodology had the smallest values, 5.3 billion GPops for *Mexican Hat* and 4.9 billion GPops for *Salutowicz*. Table 7 also presents the GPops for the evaluation in the GPU of the best individual found after the evolution is completed. The best individual GPops results are greater than the GP evolution results because the evaluation of the best individual takes considerably less time than the whole GP evolution. In addition, the GP evolution includes the overheads of creating the individuals and transferring the data to/from the GPU. For Pseudo-Assembly, the evaluation of the best individual does not consider the compilation overhead, and the GPops value obtained for the best individual is similar to that obtained by GMGP.

Figure 6 presents the speedups obtained with the Interpreter and GMGP methodologies compared to the Pseudo-Assembly methodology for the *Mexican Hat* and *Salutowicz* benchmarks. For the two benchmarks, the smallest data set generated the greatest speedups. For



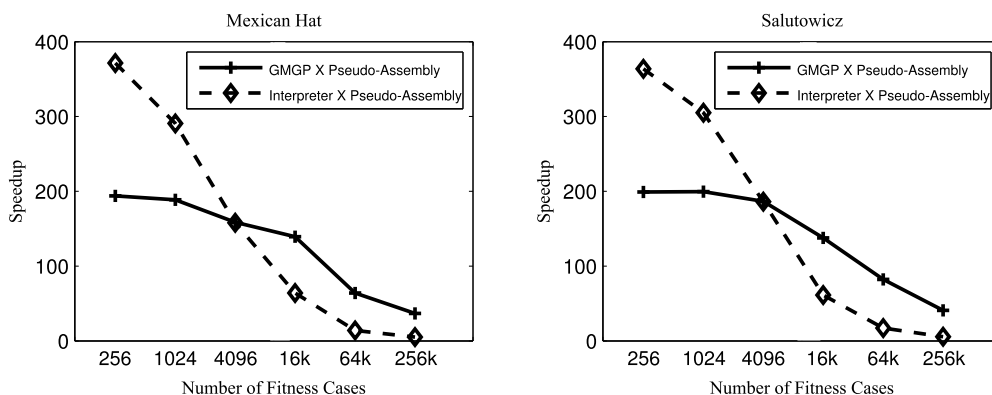


Figure 6: Speedup of Interpreter and GMGP compared to Pseudo-Assembly for the *Mexican Hat* and *Salutowicz* benchmarks with an increasing number of fitness cases.

*Mexican Hat*, Interpreter runs 371 times faster than Pseudo-Assembly, whereas GMGP runs 193 times faster than Pseudo-Assembly. The gains are similar for *Salutowicz*: Interpreter runs 363 times faster than Pseudo-Assembly, and GMGP runs 199 times faster than Pseudo-Assembly. As the problem size increases, the speedups compared to Pseudo-Assembly become smaller for both benchmarks. We will compare only Interpreter and GMGP in the remainder of this analysis.

Figure 7 presents the speedup obtained with GMGP compared to Interpreter for *Mexican Hat* and *Salutowicz*. GMGP performs better for larger data sets for both benchmarks. For the small data sets, in GMGP, the number of fitness cases used is not sufficient to compensate for the overhead of uploading the individuals, and the Interpreter methodology is faster. GMGP outperforms Interpreter for fitness case sizes exceeding 4,096. GMGP is 7.3 times faster than Interpreter for *Mexican Hat* and a fitness case size of 256K. Similar results were obtained for *Salutowicz*. As expected, GMGP is promising for applications with large data sets.

To explain why GMGP outperforms Interpreter for large data sets, we analyze the execution time breakdown for each approach in detail. Figures 8 and 9 present the execution breakdown of GMGP and Interpreter for the *Mexican Hat* and *Salutowicz* benchmarks with an increasing number of fitness cases. The execution time was broken into the same components as described in Table 6.

A comparison of GMGP's upload time from Figure 8 with Interpreter's upload time from Figure 9 indicates that it is more costly to load the GPU binary to the graphics card than to transfer the tokens through the PCIe bus. However, these times remain constant as the problem size increases. The download times for GMGP and Interpreter are almost the same, but both times increase with increasing problem size. This result is expected, as the two approaches use exactly the same data set, and the computations produce the same number of results to be copied through the PCIe bus. The result of each thread execution is one float value. The results of the threads in one block are reduced to one result in the global

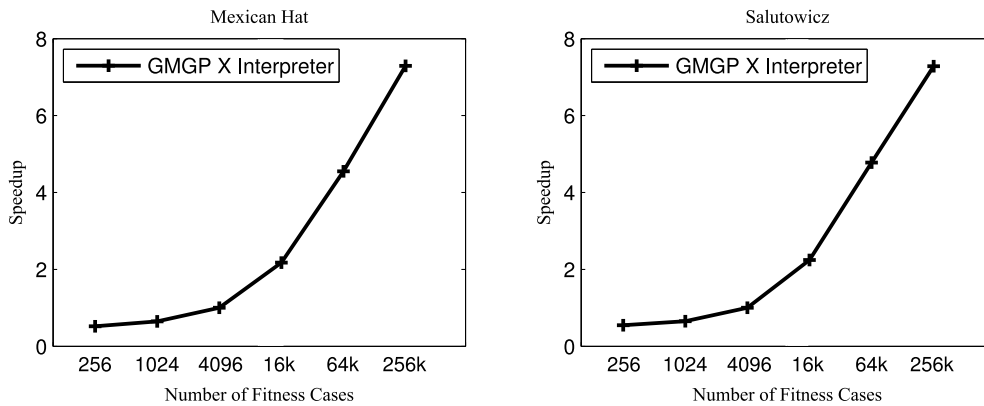


Figure 7: Speedup of GMGP compared to Interpreter for the *Mexican Hat* and *Salutowicz* benchmarks with an increasing number of fitness cases.

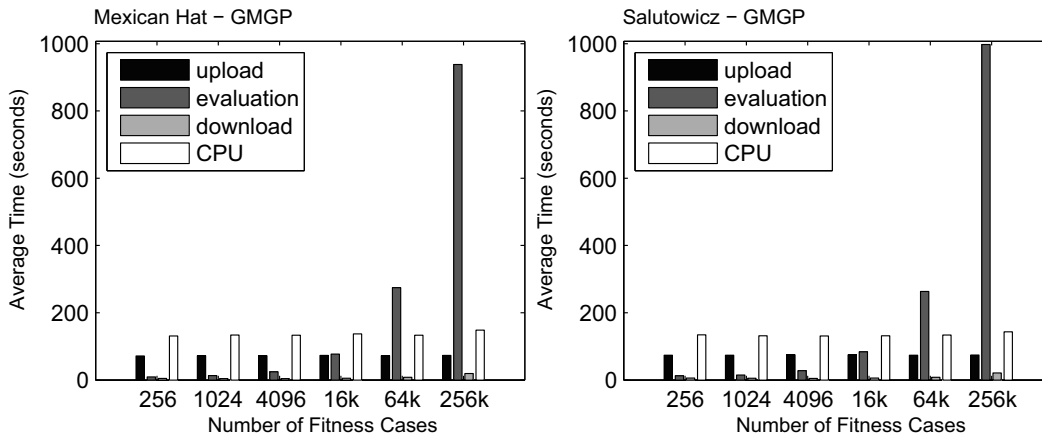


Figure 8: Execution time breakdown of GMGP. The graph presents the time broken down as follows: upload, the time spent loading the GPU binaries to the GPU memory; evaluation, the time spent computing the fitness cases; download, the time spent copying the fitness result from the GPU to the CPU; and CPU, the time during which the GP methodology is executed on the CPU.

memory. Then, the block results are reduced to one value for each individual in the CPU. The number of results transferred depends on the number of blocks used to compute all of the fitness cases. The CPU overhead has a similar behavior because the time spent running the GP methodology on the CPU is expected to be the same for GMGP and Interpreter, as the parallelized portion of the code is the evaluation function. We can compare the

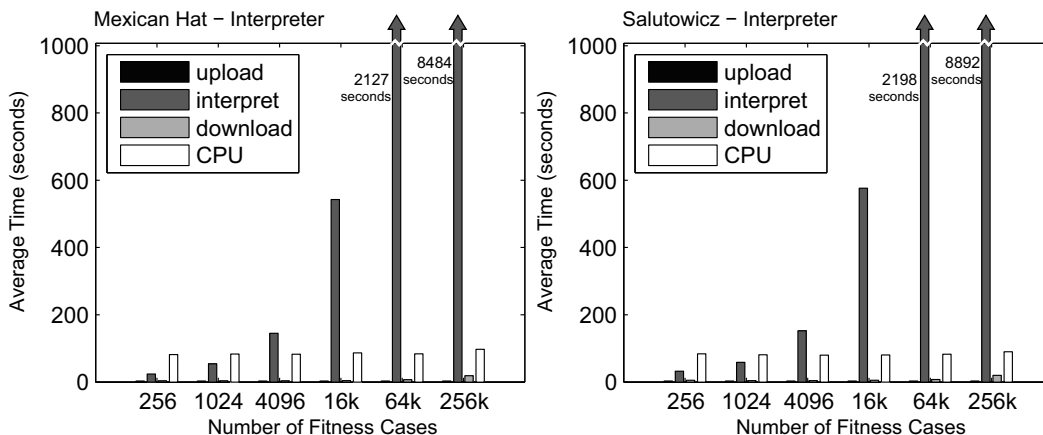


Figure 9: Execution time breakdown of Interpreter. The graph presents the time broken into: upload, the time necessary to transfer the tokens through the PCIe bus; interpret, the interpretation time; download, the time spent copying the fitness result from the GPU to the CPU; and CPU, the time during which the GP methodology is executed on the CPU.

evaluation function times for GMGP and Interpreter by comparing the `evaluation` time of Figure 8 with the `interpret` time of Figure 9. For small data sets, the `evaluation` time of GMGP is smaller than the `interpret` time of Interpreter, but the difference is small. However, as the problem size increases, the `interpret` time increases significantly because the Interpreter methodology must execute an excessive amount of additional instructions, such as comparisons and branches. For GMGP, the `evaluation` time increases slightly because it executes only the necessary GP instructions. Thus, the total time difference between GMGP and Interpreter increases for larger data sets.

#### 7.3.4 QUALITY OF RESULTS

To compare the quality of the results of the Compiler, Pseudo-Assembly, Interpreter, and GMGP methodologies on the GPU, we used the same random seed at the beginning of the first experiment of each approach. We compared the intermediate and final results. All GPU approaches produced identical results, comparing all available precision digits. The only difference among them was the execution time.

In Table 8, we analyze the results for 10 different executions of Compiler, Pseudo-Assembly, Interpreter, and GMGP. Table 8 presents the best individuals' average and standard deviation ( $\sigma$ ) for the training, validation, and testing data sets for the *Mexican Hat* and *Salutowicz* benchmarks considering 16K fitness cases. Because each experiment was repeated 10 times, the standard deviations of all cases are relatively low for the number of executions used.

Benchmark	Methodology	Training		Validation		Test	
		Average	$\sigma$	Average	$\sigma$	Average	$\sigma$
Mexican Hat	GMGP	0.046	0.007	0.048	0.008	0.053	0.008
	Interpreter	0.046	0.007	0.048	0.008	0.053	0.008
	Pseudo-Assembly	0.046	0.007	0.048	0.008	0.053	0.008
	Compiler	0.046	0.007	0.048	0.008	0.053	0.008
Salutowicz	GMGP	0.17	0.10	0.19	0.12	0.15	0.08
	Interpreter	0.17	0.10	0.19	0.12	0.15	0.08
	Pseudo-Assembly	0.17	0.10	0.19	0.12	0.15	0.08
	Compiler	0.17	0.10	0.19	0.12	0.15	0.08

Table 8: Mean Absolute Errors (MAEs) in GPU evolution for the *Mexican Hat* and *Salutowicz* benchmarks. The table presents the best individuals’ average and standard deviation ( $\sigma$ ) for the training, validation, and testing data sets for 16K fitness cases, with a precision of  $10^{-3}$ .

#### 7.4 Mackey-Glass Benchmark

The *Mackey-Glass* benchmark (Jang and Sun, 1993) is a chaotic time-series prediction benchmark, and the *Mackey-Glass* chaotic system is given by the non-linear time delay differential Equation (11).

$$\frac{dx(t)}{dt} = \frac{0.2x(t-\tau)}{1+x^{10}(t-\tau)} - 0.1x(t) \quad (11)$$

The *Mackey-Glass* system has been used as a GP benchmark in various works (Langdon and Banzhaf, 2008b,c). In our experiments, the time series consists of 1,200 data points, and GP has the task of predicting the next value when historical data are provided. The GP inputs are eight earlier values from the series, at 1, 2, 4, 8, 16, 32, 64, and 128 time steps ago.

##### 7.4.1 PARAMETER SETTINGS

The parameters used for the GP evolution in the *Mackey-Glass* benchmark are presented in Table 9. We used a small population size and a large number of generations, as previously explained. The number of generations was defined according to the number of individuals proposed by Langdon and Banzhaf (2008c).

##### 7.4.2 PERFORMANCE ANALYSIS

We analyze the performance of GMGP for the *Mackey-Glass* benchmark using the GPops metric. Table 10 presents the number of GPops obtained by GMGP. We present the GPops for the GP evolution in the GPU considering the operations spent in executing the evaluation function for all individuals and counting all non-NOP operations. GMGP obtained 77.7 billion GPops. When we consider the GP evaluation combined with the load of the

Parameter	Settings
Number of generations	512,000
Population size	20
NOP initial probability ( $\alpha_{0,0}$ )	0.9
Step size ( $s$ )	0.004
Maximum program length	128
Function set	Table 2
Set of constants	{0, 0.01, 0.02, ..., 1.27}

Table 9: Parameter settings for the *Mackey-Glass* benchmark. The number of individuals (number of population x number of generations) was defined according to the literature. The initial probability of NOP and step size were obtained in previous experiments.

	GPops
GP evolution	77.7 billion
+ loading data	8.85 billion
+ results transfer	8.4 billion
Total computation	3.59 billion
Best individual	8.6 billion

Table 10: Results of GMGP running the *Mackey-Glass* benchmark in GPops. The table presents the number of GPops spent in the GP evolution in the GPU, progressively including the overhead of loading the individuals code into GPU and transferring the results back to the CPU. At the end, we provide the results for the entire computation, including the overhead of CPU computation, and the results for the execution of the best individual.

individual code into the GPU memory, GMGP obtained 8.85 billion GPops. The load of data into the GPU memory does not include any GP operation and requires a substantial time in the evolution process. The load time is fixed regardless of the size of the data set. The idea is to amortize this cost by the faster execution of a larger data set. However, the *Mackey-Glass* benchmark has a small number of fitness cases.

For the measures that consider the transfer of the results to the CPU memory, the GPops value decreased to 8.4 billion. When the entire computation is considered, including the overhead of the CPU computation, GMGP achieved 3.59 billion GPops. At the end of the evolution, the best individual was executed, and the performance of the best individual execution was 8.6 billion GPops.

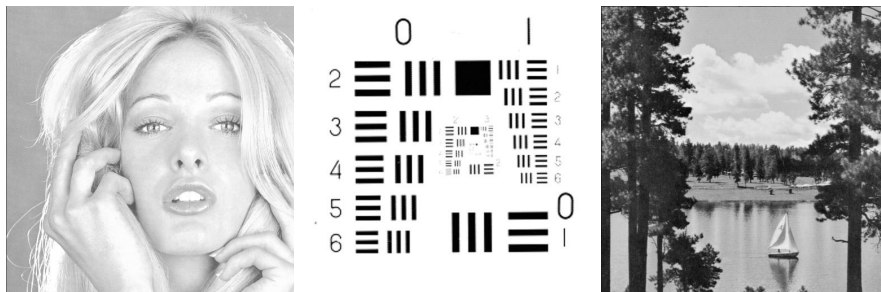


Figure 10: The three gray-scale images used for training. The image resolutions are  $512 \times 512$  pixels.

### 7.4.3 QUALITY OF THE RESULTS

The quality of the results produced by GMGP was analyzed using 10 GP executions. We computed the RMS error and standard deviation. The average error was 0.0077, and the standard deviation was 0.0021. The error is lower than the errors presented in the literature due to the difference in the GP models used. The results presented in the literature used a tree-based GP with a tree size limited to 15 and depth limited to 4. In contrast, GMGP can evolve individuals with at most 128 linear instructions. Accordingly, it was possible to find an individual that better addressed this benchmark problem.

## 7.5 Sobel filter

The *Sobel filter* is a widely used edge detection filter. Edges characterize boundaries and are therefore considered crucial in image processing. The detection of edges can assist in image segmentation, data compression, and image reconstruction. The Sobel operator calculates the approximate image gradient of each pixel by convolving the image with a pair of  $3 \times 3$  filters. These filters estimate the gradients in the horizontal ( $x$ ) and vertical ( $y$ ) directions, and the magnitude of the gradient is the sum of these gradients. All edges in the original image are greatly enhanced in the resulting image, and the slowly varying contrast is suppressed.

The evolution of an image filter uses a reverse-engineering approach, where the problem is to find the mapping between the original image and resulting image after the filter is applied (Harding and Banzhaf, 2008, 2009). The GP task is to discover the operations that transformed the input image into the filtered image. In our experiments, we used six  $512 \times 512$  images taken from the USC-SIPI image repository (Weber, 1997). The gray-scale versions of all 6 images and the resulting images after the *Sobel filter* were computed using the GIMP image processing tool (GIMP, 2008). Figure 10 presents the three gray-scale images used for training. Figure 11 shows the two images used for validation. Figure 12 shows, for the same image, the original image in gray scale, the resulting image after the *Sobel filter* is applied by the GIMP tool, and the output image produced by the GMGP evolved filter.



Figure 11: The two gray-scale images used for validation. The image resolutions are  $512 \times 512$  pixels.

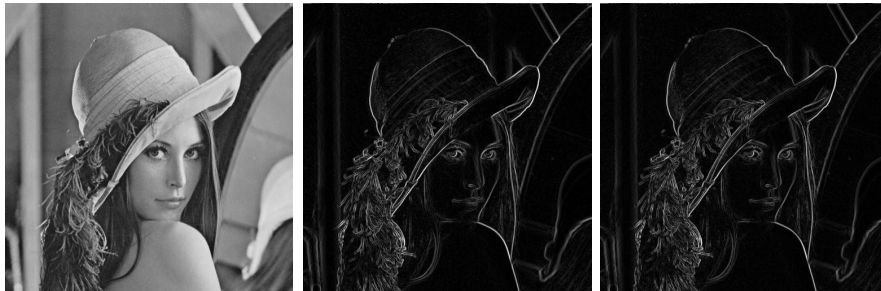


Figure 12: Results of evolving the filter for one test image. The leftmost image is the original gray-scale test image. The center image is the output image produced by applying the GIMP Sobel filter. The rightmost image is the output image produced by the GMGP evolved filter.

#### 7.5.1 PARAMETER SETTINGS

The parameters used for the GP evolution of the *Sobel filter* are presented in Table 11. The population size also employs a low number of individuals for the reasons explained before. The number of generations, NOP initial probability, step size, and maximum program length were obtained from previous experiments.

#### 7.5.2 PERFORMANCE ANALYSIS

The performance of the *Sobel filter* in GPops is presented in Table 12. Considering only the GPU evaluation of all non-NOP instructions, GMGP achieved 287.3 billion GPops. When the overhead of uploading the GPU binaries is included, the GPops are reduced to 274.2 billion. The reduction in GPops was less pronounced because this problem has a larger data set that compensates for the initial overhead of loading the program. When we include the overhead

Parameter	Settings
Number of generations	400,000
Population size	20
NOP initial probability ( $\alpha_{0,0}$ )	0.9
Step size ( $s$ )	0.001
Maximum program length	128
Function set	Table 2
Set of constants	{1,2,3,4,5,6,7,8,9}

Table 11: Parameter settings for the *Sobel filter*. The values of the number of generations, population size, initial probability of NOP, and step size were obtained in previous experiments.

	GPods
GP evolution	287.3 billion
+ loading data	274.2 billion
+ results transfer	268.6 billion
Total computation	249.9 billion
Best individual	295.8 billion

Table 12: Results of GMGP running the *Sobel filter* in GPods. The table presents the number of GPods spent in the GP evolution in the GPU, progressively including the overheads of loading the individual code into the GPU and transferring the results back to the CPU. At the end, we present the results for the entire computation, including the overhead of CPU computation, and the results for the execution of the best individual.

of transferring the results back to the CPU through the PCIe bus, GMGP obtained 268.6 billion GPods. When the entire computation is considered, including the overhead of the CPU computation during the evolution, GMGP obtained 249.9 billion GPods. After the evolution, the best individual was executed on the GPU, and we calculated a performance of 295.8 billion GPods for the best individual.

### 7.5.3 QUALITY OF THE RESULTS

The quality of the results produced by GMGP for the *Sobel filter* was analyzed with 10 GP runs. We computed the MAE and standard deviation. Table 13 presents both the MAEs and standard deviations for the training, validation, and testing data sets. The errors are low compared to those presented in literature because our GP parameters were set to provide a better-quality evolved filter. The quality of the *Sobel filter* evolved by GMGP can also be assessed visually. The image presented at the right of Figure 12 was produced by the



Training		Validation		Test	
Average	$\sigma$	Average	$\sigma$	Average	$\sigma$
2.11	0.61	2.21	0.64	2.03	0.599

Table 13: MAEs in GMGP evolution for the *Sobel filter*. The table presents the average and standard deviation ( $\sigma$ ) of the best individual for the training, validation, and testing data sets.

best individual of GMGP applied to the test image. This image can be visually compared to the image in the center of Figure 12, which was obtained using the *Sobel filter* of GIMP. A visual comparison of these two images indicates that the evolved filter produced an image with more prominent horizontal edges without significantly increasing the noise.

## 7.6 20-bit Boolean Multiplexer

The Boolean instructions of GMGP were evaluated using the *20-bit Boolean Multiplexer* benchmark (Langdon, 2010b, 2011). In the *20-bit Boolean Multiplexer* benchmark, there are 1,048,576 possible combinations of 20 arguments of a 20-bit Multiplexer. In our experiments, we used 1,048,576 fitness cases to evaluate all of the individuals, which is possible because GMGP evaluates each individual rapidly. This experiment is the first time this benchmark has been solved in this manner, using all fitness cases. The bit-level parallelism was exploited by performing bitwise operations over a 32-bit integer that packs 32 Boolean fitness cases.

### 7.6.1 PARAMETER SETTINGS

The parameter settings used for the *20-bit Boolean Multiplexer* benchmark are presented in Table 14. More individuals were used in the population than in the previous benchmark experiments reported in this paper. This problem addresses more input variables and a larger data set. The number of generations was computed to produce a total number of individuals similar to the numbers presented in the literature. However, the zero error solution was found before the maximum number of generations was reached for all 10 GP executions. The maximum program length was obtained by verifying the minimum length needed to solve this problem benchmark.

### 7.6.2 PERFORMANCE ANALYSIS

Table 15 presents the number of GPops obtained by GMGP for the GP evolution in the GPU (execution of the evaluation of all individuals considering the non-NOP operations); the GP evolution including the loading of the individual code into the GPU memory; the GP evolution, including the loading of the individuals and the transfer of the results to the CPU memory; the total computation, including the CPU computation; and the best individual computation.

Table 15 illustrates that GMGP obtained 5.88 trillion GPops when evaluating the individuals. When the load of the individuals is considered, a value of 5.24 trillion GPops was obtained. This benchmark has a large data set. The amount of computation is sufficient to

Parameter	Settings
Number of generations	First Solution or 14,000,000
Population size	40
NOP initial probability ( $\alpha_{0,0}$ )	0.9
Step size ( $s$ )	0.004
Maximum program length	512
Function set	Table 3
Set of constants	–

Table 14: Parameter settings for the *20-bit Boolean Multiplexer*. The values of the number of generations, population size, initial probability of NOP, and maximum program length were obtained in previous experiments, where we varied the values until the problem was solved.

	GPops
GP evolution	5.88 trillion
+ loading data	5.24 trillion
+ results transfer	5.19 trillion
Total computation	2.74 trillion
Best individual	4.87 trillion

Table 15: Results of GMGP running the *20-bit Boolean Multiplexer* benchmark in GPops. The table presents the number of GPops spent in the GP evolution in the GPU, progressively including the overhead of loading the individual code into GPU and transferring the results back to the CPU. At the end, we present the results for the entire computation, including the overhead of CPU computation, and the results for the execution of the best individual.

amortize the load time. Thus, the total number of GPops is not degraded with the inclusion of the load of individuals. When the results transfer is included, the results remain almost the same, and GMGP achieves 5.19 trillion GPops. When the CPU overhead is considered, the performance is reduced to 2.74 trillion GPops. This result suggests that porting the whole GP evolution algorithm to run in the GPU (not only the evaluation function), could significantly improve the overall performance. The execution of the GMGP’s best individual achieved 4.87 trillion GPops.

Experiment	Generation	Total Number of Individuals
1	2,413,505	96,540,200
2	1,246,979	49,879,160
3	3,238,394	129,535,760
4	7,802,509	312,100,360
5	8,892,873	355,714,920
6	10,737,990	429,519,600
7	5,255,728	210,229,120
8	2,576,655	103,066,200
9	5,469,381	218,775,240
10	3,395,730	135,829,200

Table 16: Generation at which GMGP solved the *20-bit Boolean Multiplexer* and the total number of individuals used in the evolution. The population size is 40 individuals.

### 7.6.3 QUALITY OF THE RESULTS

GMGP was able find the zero solution for the *20-bit Boolean Multiplexer* benchmark before the maximum number of generations was reached for all 10 GP executions. Table 16 presents the number of generations and total number of individuals needed to find this solution.

## 8. Discussions

It is difficult to compare our quantum-inspired LGP timings to the timings of the tree-based implementations of GP in GPU proposed in the literature. They used different individual representations and different evolutionary algorithms. However, we can compare the GPops results. For the *Mackey-Glass* benchmark, on the GTX TITAN, we obtained up to 3.59 billion GPops when considering the entire evaluation (GPU and CPU) and 77.7 billion GPops when considering only the GPU processing. Langdon and Banzhaf (2008c) obtained 895 million GPops for this benchmark. However, we used a larger individual than Langdon and Banzhaf (2008c) to achieve a more accurate prediction result (smaller RMS error). We obtained up to 249.9 billion GPops considering the whole evaluation (GPU and CPU) and 287.3 billion GPops considering only the GPU processing for the *Sobel filter* benchmark. The *Sobel filter* was also evolved, along with other filters, by Harding and Banzhaf (2008). They obtained an average of 145 million GPops and a peak performance of 324 million GPops. Harding and Banzhaf (2009) attained on average 4.21 billion GPops when evolving the same type of filter. They used Cartesian GP and a cluster of 16 workstations to compile the code. For the *20-bit Boolean Multiplexer* benchmark, we obtained up to 2.74 trillion GPops considering the entire evaluation and 5.88 trillion GPops considering only the GPU processing. Langdon (2010b) obtained up to 254 billion GPops in the entire evaluation process (CPU and GPU) for a 37-bit Boolean multiplexer. The literature provides other results for different benchmarks. Recently, Langdon (2010a) obtained 8.5 billion GPops for a bioinformatics data mining problem.

Despite the highly data-parallel nature of the GP problems that we considered, we could achieve 336.3 GFLOPs of execution in the GTX TITAN, whose peak performance is 4,500 GFLOPs, running the *Sobel filter* benchmark. The peak performance of the GPU is measured using the FMA instruction, which is not present in our function set. Furthermore, it is difficult to reach the peak single precision performance even for embarrassingly parallel applications, such as SGEMM (Lai and Seznec, 2013). The main obstacles for GMGP in achieving the peak performance are: (i) it includes more complicated floating-point operations like divisions, sine, cosine, and square root, that take several cycles to execute; (ii) it includes a reduction operation that requires synchronization; (iii) the small population size makes the overhead of uploading the individuals to the GPU memory more significant.

## 9. Conclusions

In this work, we proposed a new methodology to parallelize the evaluation process on the GPU called **GMGP**. Our methodology is inspired by quantum computing and includes the principles of the quantum bit and the superposition of states, which increases the diversity of a quantum population. In addition, GMGP is the first methodology to generate individuals using the GPU machine code instead of compiling or interpreting them. We eliminate the compilation time overhead without including the parsing of the code and divergence required for the interpretation. The parallelism is exploited at two levels in the evaluation process, i.e., at the individual level and at the fitness case level. This parallelization scheme guarantees adequate scalability as the number of cores in the GPU increases.

To compare GMGP to other GP methodologies for GPUs found in the literature, we implemented three different LGP-based and quantum-inspired approaches: (i) *compilation* (Compiler), which generates the individuals in GPU code and requires compilation; (ii) *pseudo-assembly* (Pseudo-Assembly), which generates the individuals in an intermediary assembly code and also requires compilation; and (iii) *interpretation* of multiple programs (Interpreter), which interprets the codes and does not require compilation. Our results demonstrated that GMGP outperformed all of the previous methodologies for the larger data sets of the *Mexican Hat* and *Salutowicz* benchmarks. The maximum speedups obtained were 827.7 against Compiler, 199 against Pseudo-Assembly and 7.3 against Interpreter. In terms of the GPops, for the entire evolution (GPU and CPU), GMGP achieved approximately 200.5 billion GPops for the *Mexican Hat* and *Salutowicz* benchmarks, 3.59 billion GPops for the *Mackey-Glass* benchmark, 249.9 billion GPops for the *Sobel filter* benchmark, and 2.74 trillion GPops for the *20-bit Boolean Multiplexer* benchmark.

These results provide a new perspective on GPU-based implementations of GP. Our methodology is scalable and introduces the possibility of addressing large problems within a reasonable period of time. We were the first to evolve the *20-bit Boolean Multiplexer* problem using all of the fitness cases during the evolution. The largest evolved Multiplexer that used all fitness cases in the evolution used only 11 bits, whereas the others used samples to evolve larger problems.

In our future work, we intend to develop a GP evolutionary model to run entirely in the GPU, which would offer two advantages. First, the GP model would run faster after being parallelized to GPUs. Second, we would eliminate the overhead associated with copying

the fitness results from the GPU to the CPU through the PCIe bus, yielding considerable speedups.

## Acknowledgments

We would like to acknowledge support for this project from the National Counsel of Technological and Scientific Development (CNPq) and the Carlos Chagas Filho Research Support Foundation (FAPERJ).

## References

- Fawzan S. Alfares and Ibrahim I. Esat. Real-coded quantum inspired evolution algorithm applied to engineering optimization problems. In *Second International Symposium on Leveraging Applications of Formal Methods, Verification and Validation, ISoLA 2006*, pages 169–176. IEEE, 2006.
- David Andre and John R. Koza. *Parallel Genetic Programming: a Scalable Implementation Using the Transputer Network Architecture*, in collection 16, pages 317–338. MIT Press, Cambridge, MA, USA, 1996.
- Wolfgang Banzhaf, Peter Nordin, Robert E Keller, and Frank D Francone. *Genetic Programming: an Introduction: on the Automatic Evolution of Computer Programs and its Applications*. The Morgan Kaufmann Series in Artificial Intelligence. Morgan Kaufmann Publishers, 1997.
- Forrest H Bennett III, John R. Koza, James Shipman, and Oscar Stiffelman. Building a parallel computer system for \$18,000 that performs a half peta-flop per day. In *Proceedings of the Genetic and Evolutionary Computation Conference*, volume 2, pages 1484–1490, Orlando, Florida, USA, 1999. Morgan Kaufmann.
- Markus Brameier and Wolfgang Banzhaf. *Linear Genetic Programming*. Genetic and Evolutionary Computation. Springer-Verlag, 2007.
- Jens Busch, Jens Ziegler, Christian Aue, Andree Ross, Daniel Sawitzki, and Wolfgang Banzhaf. Automatic generation of control programs for walking robots using genetic programming. In *Genetic Programming*, pages 258–267. Springer, 2002.
- Darren M Chitty. A data parallel approach to genetic programming using programmable graphics hardware. In *Proceedings of the 9th Annual Conference on Genetic and Evolutionary Computation*, pages 1566–1573. ACM, 2007.
- Leandro F. Cupertino, Cleomar P. Silva, Douglas M. Dias, Marco A. C. Pacheco, and Cristiana Bentes. Evolving CUDA PTX programs by quantum inspired linear genetic programming. In *Proceedings of the 13th Annual Conference Companion on Genetic and Evolutionary Computation*, pages 399–406. ACM, 2011.
- Douglas M. Dias and Marco A. C. Pacheco. Toward a quantum-inspired linear genetic programming model. In *Congress on Evolutionary Computation*, pages 1691–1698, 2009.

- Douglas M. Dias and Marco A. C. Pacheco. Quantum-inspired linear genetic programming as a knowledge management system. *The Computer Journal*, 56(9):1043–1062, 2013.
- Amer Draa, Souham Meshoul, Hichem Talbi, and Mohamed Batouche. A quantum inspired differential evolution algorithm for rigid image registration. In *Proceedings of the International Conference on Computational Intelligence, Istanbul*, pages 408–411, 2004.
- GNU GIMP. Image manipulation program. *User Manual, Edge-Detect Filters, Sobel, The GIMP Documentation Team*, 2008.
- Kuk-Hyun Han and Jong-Hwan Kim. Quantum-inspired evolutionary algorithm for a class of combinatorial optimization. *IEEE Transactions on Evolutionary Computation*, 6(6):580–593, 2002.
- Simon Harding and Wolfgang Banzhaf. Fast genetic programming on GPUs. In *Genetic Programming*, volume 4445 of *Lecture Notes in Computer Science*, pages 90–101. Springer, 2007.
- Simon Harding and Wolfgang Banzhaf. Genetic programming on GPUs for image processing. *International Journal of High Performance Systems Architecture*, 1(4):231–240, 2008.
- Simon L. Harding and Wolfgang Banzhaf. Distributed genetic programming on GPUs using CUDA. In *Workshop on Parallel Architectures and Bioinspired Algorithms*, Raleigh, USA, 2009.
- Jyh-Shing Roger Jang and Chuen-Tsai Sun. Predicting chaotic time series with fuzzy if-then rules. In *Second IEEE International Conference on Fuzzy Systems*, pages 1079–1084. IEEE, 1993.
- John R. Koza. *Genetic Programming: on the Programming of Computers by Means of Natural Selection*. The MIT press, 1992.
- John R. Koza. *Genetic Programming II: Automatic Discovery of Reusable Programs*. The MIT press, 1994.
- Junjie Lai and André Sez nec. Performance upper bound analysis and optimization of SGEMM on Fermi and Kepler GPUs. In *International Symposium on Code Generation and Optimization, CGO'13*, pages 1–10. IEEE Computer Society, 2013.
- William B. Langdon. Large scale bioinformatics data mining with parallel genetic programming on graphics processing units. In Francisco Fernández Vega and Erick Cantú-Paz, editors, *Parallel and Distributed Computational Intelligence*, volume 269 of *Studies in Computational Intelligence*, pages 113–141. Springer Berlin Heidelberg, 2010a.
- William B. Langdon. A many threaded CUDA interpreter for genetic programming. In *Proceedings of the 13th European Conference on Genetic Programming, EuroGP'10*, pages 146–158, Berlin, Heidelberg, 2010b. Springer-Verlag.

- William B. Langdon. Minimising testing in genetic programming. Technical Report RN/11/10, University College London, April 2011.
- William B. Langdon and Wolfgang Banzhaf. A SIMD interpreter for genetic programming on GPU graphics cards. In *Genetic Programming*, volume 4971 of *Lecture Notes in Computer Science*, pages 73–85. Springer, 2008a.
- William B. Langdon and Wolfgang Banzhaf. Repeated patterns in genetic programming. *Natural Computing*, 7(4):589–613, 2008b.
- William B. Langdon and Wolfgang Banzhaf. A SIMD interpreter for genetic programming on GPU graphics cards. In *Proceedings of the 11th European Conference on Genetic Programming*, EuroGP’08, pages 73–85, Berlin, Heidelberg, 2008c. Springer-Verlag.
- William B. Langdon and M. Harman. Evolving a CUDA kernel from an nVidia template. In *IEEE Congress on Evolutionary Computation*, pages 1–8, 2010.
- William B. Langdon and A. Harrison. GP on SPMD parallel graphics hardware for mega bioinformatics data mining. *Soft Computing - A Fusion of Foundations, Methodologies and Applications*, 12:1169–1183, 2008.
- Benjamin P Lanyon, Marco Barbieri, Marcelo P. Almeida, Thomas Jennewein, Timothy C. Ralph, Kevin J. Resch, Geoff J. Pryde, Jeremy L. O’Brien, Alexei Gilchrist, and Andrew G. White. Quantum computing using shortcuts through higher dimensions. *Nature Physics* 5, 134 (2009), 2008.
- Tony E. Lewis and George D. Magoulas. Identifying similarities in TMBL programs with alignment to quicken their compilation for GPUs: computational intelligence on consumer games and graphics hardware. In *Proceedings of the 13th Annual Conference Companion on Genetic and Evolutionary Computation*, pages 447–454. ACM, 2011.
- Mark Moore and Ajit Narayanan. Quantum-inspired computing. Research report 341, Department of Computer Science, University of Exeter, 1995.
- Peter Nordin. AIMGP: A formal description. In *Late Breaking Papers at the Genetic Programming 1998 Conference*, University of Wisconsin, Madison, WI, USA, 1998. Stanford University Bookstore.
- Nvidia. *CUDA C Programming Guide: Design Guide*. Nvidia Corporation, July 2013. Manual ID: PG-02829-001\_v5.5.
- Mihai Oltean, Crina Groşan, Laura Dioşan, and Cristina Mihăilă. Genetic programming with linear representation: a survey. *International Journal on Artificial Intelligence Tools*, 18(02):197–238, 2009.
- Jonathan Page, Riccardo Poli, and William B. Langdon. Smooth uniform crossover with smooth point mutation in genetic programming: a preliminary study. In *Second European Workshop on Genetic Programming*, pages 39–48, London, UK, 1999. Springer-Verlag.

- Michaël Defoin Platel, Stefan Schliebs, and Nikola Kasabov. Quantum-inspired evolutionary algorithm: a multimodel EDA. *IEEE Transactions on Evolutionary Computation*, 13(6): 1218–1232, 2009.
- Riccardo Poli, William B. Langdon, and Nicholas Freitag McPhee. *A Field Guide to Genetic Programming*. Published via <http://lulu.com>, 2008. (contributions by J. R. Koza).
- Petr Pospichal, Eoin Murphy, Michael O’Neill, Josef Schwarz, and Jiri Jaros. Acceleration of grammatical evolution using graphics processing units: computational intelligence on consumer games and graphics hardware. In *Proceedings of the 13th Annual Conference Companion on Genetic and Evolutionary Computation*, pages 431–438. ACM, 2011.
- Denis Robilliard, Virginie Marion, and Cyril Fonlupt. High performance genetic programming on GPU. In *Proceedings of the 2009 Workshop on Bio-Inspired Algorithms for Distributed Systems*, BADS ’09, pages 85–94, New York, NY, USA, 2009. ACM.
- Abdel Salhi, Hugh Glaser, and David De Roure. Parallel implementation of a genetic-programming based tool for symbolic regression. *Information Processing Letters*, 66(6): 299–307, 1998.
- Luciano R. Silveira, Ricardo Tanscheit, and Marley Vellasco. Quantum-inspired genetic algorithms applied to ordering combinatorial optimization problems. In *IEEE Congress on Evolutionary Computation (CEC)*, pages 1–7, 2012.
- Walter A. Tackett. Genetic programming for feature discovery and image discrimination. In *Proceedings of the 5th International Conference on Genetic Algorithms, ICGA-93*, pages 303–309, 1993.
- Hichem Talbi, Mohamed Batouche, and Amer Draa. A quantum-inspired evolutionary algorithm for multiobjective image segmentation. *International Journal of Mathematical, Physical and Engineering Science*, 1(2):109–114, 2007.
- Ian Turton, Stan Openshaw, and Gary Diplock. Some geographic applications of genetic programming on the Cray T3D supercomputer. In *UK Parallel’96*, pages 135–150, University of Surrey, 1996. Springer.
- Ekaterina J Vladislavleva, Guido F Smits, and Dick Den Hertog. Order of nonlinearity as a complexity measure for models generated by symbolic regression via pareto genetic programming. *IEEE Transactions on Evolutionary Computation*, 13(2):333–349, 2009.
- Allan G. Weber. The USC-SIPI image database. Technical report, University of Southern California, Signal and Image Processing Institute, Department of Electrical Engineering, Los Angeles, CA 90089-2564 USA, 3740 McClintock Ave, October 1997.
- Garnett Wilson and Wolfgang Banzhaf. Linear genetic programming GPGPU on Microsoft’s Xbox 360. In *Congress on Evolutionary Computation*, pages 378–385, 2008.
- Gexiang Zhang. Quantum-inspired evolutionary algorithms: a survey and empirical study. *Journal of Heuristics*, 17(3):303–351, June 2011.